The Canadian Mineralogist
Vol. 53, pp. 401-428 (2015)
DOI: 10.3749/canmin.1400044

FROM STRUCTURE TOPOLOGY TO CHEMICAL COMPOSITION. XVIII. TITANIUM SILICATES: REVISION OF THE CRYSTAL STRUCTURE AND CHEMICAL FORMULA OF BETALOMONOSOVITE, A GROUP-IV TS-BLOCK MINERAL FROM THE LOVOZERO ALKALINE MASSIF, KOLA PENINSULA, RUSSIA

ELENA SOKOLOVA[§], YASSIR ABDU, AND FRANK C. HAWTHORNE

Department of Geological Sciences, University of Manitoba, 125 Dysart Road, Winnipeg, Manitoba R3T 2N2, Canada

ALESSANDRO GENOVESE

Istituto Italiano di Tecnologia, Via Morego 30, 16163 Genova, Italy

FERNANDO CÁMARA

Dipartimento di Scienze della Terra, Università degli Studi di Torino, via Valperga Caluso 35, 10125 Torino, Italy

ALEXANDER P. KHOMYAKOV**

Institute of Mineralogy, Geochemistry and Crystal Chemistry of Rare Elements, Veresaev Street 15, Moscow 121357, Russia

ABSTRACT

The crystal structure of betalomonosovite, ideally $Na_6\square_4Ti_4(Si_2O_7)_2[PO_3(OH)][PO_2(OH)_2]O_2(OF)$, *a* 5.3331(7), *b* 14.172 (2), *c* 14.509(2) Å, α 103.174(2), β 96.320(2), γ 90.278(2)°, *V* 1060.7(4) Å^3, from the Lovozero alkaline massif, Kola peninsula, Russia, has been refined in the space group $P\bar{1}$ to R = 6.64% using 3379 observed ($F_o > 4\sigma F$) reflections collected with a single-crystal APEX II ULTRA three-circle diffractometer with a rotating-anode generator (Mo$K\alpha$), multilayer optics, and an APEX-II 4K CCD detector. Electron-microprobe analysis gave the empirical formula $(Na_{5.39}Ca_{0.36}Mn_{0.04}Mg_{0.01})_{\Sigma 5.80}(Ti_{2.77}Nb_{0.48}Mg_{0.29}Fe^{3+}_{0.23}Mn_{0.20}Zr_{0.02}Ta_{0.01})_{\Sigma 4}(Si_{2.06}O_7)_2[P_{1.98}O_5(OH)_3]O_2[O_{0.82}F_{0.65}(OH)_{0.53}]_{\Sigma 2}$, $D_{calc.}$ = 2.969 g cm^{-3}, Z = 2, calculated on the basis of 26 (O + F) *apfu*, with H_2O determined from structure refinement. The crystal structure of betalomonosovite is characterized by extensive cation and anion disorder: more than 50% of cation sites are partly occupied. The crystal structure of betalomonosovite is a combination of a titanium silicate (TS) block and an intermediate (**I**) block. The TS block consists of HOH sheets (H-heteropolyhedral, O-octahedral) and exhibits linkage and stereochemistry typical for Group IV (Ti + Mg + Mn = 4 *apfu*) of the TS-block minerals. The **I** block is a framework of Na polyhedra and P tetrahedra which ideally gives $\{Na_2\square_4[PO_3(OH)][PO_2(OH)_2]\}$ *pfu*. Betalomonosovite is an Na-poor OH-bearing analogue of lomonosovite, $Na_{10}Ti_4(Si_2O_7)_2(PO_4)_2O_4$. In the betalomonosovite structure, there is less Na in the **I** block and in the TS block when compared to the lomonosovite structure. The OH groups occur mainly in the **I** block where they coordinate P and Na atoms and in the O sheet of the TS block (minor). The presence of OH groups in the **I** block and in the TS block is supported by IR spectroscopy and bond-valence calculations on anions. High-resolution TEM of lomonosovite shows the presence of pervasive microstructural intergrowths, accounting for the presence of signals from H_2O in the infrared spectrum of anhydrous lomonosovite. More extensive lamellae in betalomonosovite suggest a topotactic reaction from lomonosovite to betalomonosovite.

Keywords: betalomonosovite, TS-block, crystal structure, chemical formula, FTIR spectroscopy, Raman spectroscopy, transmission electron microscopy, EMP analysis.

§ *Corresponding author e-mail address*: elena_sokolova@umanitoba.ca

** *Dr. Alexander Khomyakov was involved in this work which started in the spring of 2011; he passed away on 12 October 2012 after a long illness.*

Introduction

Gerasimovskiy & Kazakova (1962) described betalomonosovite, $Na_2Ti_2Si_2O_9{\cdot}(Na,H)_3PO_4$, from the Lovozero alkaline massif, Kola Peninsula, Russia, as an intermediate member of the series lomonosovite, $Na_{10}Ti_4(Si_2O_7)_2(PO_4)_2O_4$, – murmanite, $Na_4Ti_4(Si_2O_7)_2O_4(H_2O)_4$. The crystal structure of betalomonosovite was solved by Rastsvetaeva *et al.* (1975) and then refined by Rastsvetaeva (1986, 1988) and Khalilov (1990). However, agreement between the crystal structure and the chemical analysis has never been reached. The problems with the crystal structure of betalomonosovite arise from the poor quality of its crystals, which is related to the extensive cation and anion disorder present in the structure (including H_2O). The position of H_2O in the crystal structure is still not clear (see Previous Work below). In the IMA list of minerals, betalomonosovite had been considered a discredited (D = discredited, M. Pasero, pers. commun. 2014) mineral species, with the formula $(Na,Ca)_2(Ti,Nb)_2(Si_2O_7)O(OH,F)_2{\cdot}Na[PO_2(OH)_2]$ modified after Khalilov (1990). The latter formula is irreconcilable with the structure, and an ideal stoichiometry has not been derived. In 2013, betalomonosovite disappeared from the IMA list.

Betalomonosovite is a TS-block mineral in accord with Sokolova (2006), who divided Ti-disilicate minerals into four groups, characterized by a different topology and stereochemistry of the titanium silicate (TS) block associated with different content of Ti (+ Nb + Zr + Fe^{3+} + Mg + Mn). In Groups I, II, III, and IV, Ti (+ Nb + Zr + Fe^{3+} + Mg + Mn) equals 1, 2, 3, and 4 *apfu* (atoms per formula unit), respectively. The TS block consists of the central O (trioctahedral) sheet and two H (heteropolyhedral) sheets containing Si_2O_7 groups. Each group of structures has a different linkage of H and O sheets in the TS block and a different arrangement of Ti (+ Nb + Zr + Fe^{3+} + Mg + Mn) polyhedra. Since Sokolova (2006), there has been extensive work on the TS-block minerals: revision of the crystal structure and chemical formula of delindeite (Sokolova & Cámara 2007); determination of the crystal structures of bornemanite and nechelyustovite (Cámara & Sokolova 2007, 2009); refinement of the crystal structure and revision of the chemical formula of mosandrite (Bellezza *et al.* 2009, Sokolova & Hawthorne 2013); description of the following new minerals and their crystal structures: cámaraite (Sokolova *et al.* 2009a, Cámara *et al.* 2009), schöllerite (Chukanov *et al.* 2011, Rastsvetaeva *et al.* 2011, Sokolova *et al.* 2013), lileyite (Chukanov *et al.* 2012), kazanskyite (Cámara *et al.* 2012), kolskyite (Cámara *et al.* 2013), saamite (Cámara *et al.* 2014), emmerichite (Chukanov *et al.* 2013, Aksenov *et al.* 2014), and bobshannonite (Sokolova *et al.* 2014); revision of the chemical formula and crystal chemistry of barytolamprophyllite (Sokolova & Cámara 2008) and innelite (Sokolova *et al.* 2011); and structure work on an orthorhombic polytype of nabalamprophyllite (Sokolova & Hawthorne 2008a), nacareniobsite-(Ce) (Sokolova & Hawthorne 2008b), jinshajiangite (Sokolova *et al.* 2009b), lomonosovite and murmanite (Cámara *et al.* 2008), and rinkite (Cámara *et al.* 2011). Sokolova & Cámara (2013, 2014) further developed the crystal chemistry of the TS-block minerals: they reviewed crystal chemistry for 34 minerals and introduced the new concept of basic and derivative TS-block structures.

In the crystal structure of betalomonosovite, the TS block has the stereochemistry and topology of Group IV, where Ti (+ Mg + Mn) = 4 *apfu*. In Group IV, the TS block exhibits linkage 3, where the Si_2O_7 groups of two H sheets link to the edges of two Ti octahedra of the O sheet along $\mathbf{t}_1$ ($t_1 \sim 5.4$ Å). Other Group IV minerals are as follows: murmanite, kolskyite, schöllerite, lomonosovite, quadruphite, polyphite, and sobolevite (Table 1).

We consider betalomonosovite a valid TS-block mineral of Group IV. Based on our work, betalomonosovite, $Na_6\square_4Ti_4(Si_2O_7)_2[PO_3(OH)][PO_2(OH)_2]O_2(OF)$, has been re-approved by the Commission on New Minerals, Nomenclature and Classification (CNMNC) (Nomenclature Voting Proposal 14-J, 2015). Here we report the revised crystal structure and ideal structural formula of betalomonosovite, compare the infrared spectra of betalomonosovite and lomonosovite, and compare the microstructure of both minerals using high-resolution transmission electron microscopy (HRTEM).

Previous Work

Gerasimovskiy & Kazakova (1962) described betalomonosovite, $Na_2Ti_2Si_2O_9{\cdot}(Na,H)_3PO_4$, a new mineral from the Lovozero alkaline massif, Kola Peninsula, Russia, as an intermedate member of the series lomonosovite, $Na_{10}Ti_4(Si_2O_7)_2(PO_4)_2O_4$, – murmanite, $Na_4Ti_4(Si_2O_7)_2O_4(H_2O)_4$. Gerasimovskiy & Kazakova (1962) reported a chemical analysis and the results of thermal analysis. They noted that Gerasimovskiy had identified betalomonosovite in 1938, and T.A. Burova analyzed the mineral using wet chemistry in 1939; the latter composition is given in Gerasimovskiy & Kazakova (1962). Hence betalomonosovite, known from 1938, was studied by other authors prior to its official description as a new mineral. Semenov *et al.* (1961) reported a chemical analysis for betalomonosovite from the Lovozero alkaline massif under the name of "*metalomonosovite*" and suggested two types of ideal chemical formula: (1) $Na_5H_3\mathit{MnTi}_3[Si_4P_2O_{24}]$ or $Na_5\mathit{MnTi}_3[Si_4P_2O_{21}(OH)_3]$, $Z = 1$ where Mn = Mn, Fe, Mg; Ti = Ti, Nb, Zr; and (2) $Na_2\mathit{MnTi}_3Si_4O_{16}{\cdot}2Na_{1.5}H_{1.5}PO_4$. Belov & Organova (1962) discussed the crystal chemistry of the lomonosovite group and considered betalomonosovite with

TABLE 1. IDEAL STRUCTURAL FORMULAE* AND UNIT-CELL PARAMETERS FOR GROUP-IV TS-BLOCK MINERALS

Mineral Structure type**	Ideal structural formula							*a* (Å)	*b* (Å)	*c* (Å)	α (°)	β (°)	γ (°)	Sp.gr.	*Z*	Ref.
	TS block						**I** block									
	$2A^{P}$	$2M^{H}$	$2M^{O}(1)$	$2M^{O}(2)$	$(Si_2O_7)_2X^{O}_4$	$X^{P}_{2\text{-}4}$										
murmanite B1(GIV)	Na_2	Ti_2	Ti_2	Na_2	$(Si_2O_7)_2O_4$	$(H_2O)_4$	absent	5.3875	7.0579	12.1764	93.511	107.943	90.093	$P\bar{1}$	1	(1)
kolskyite*** B7(GIV)		Ti_2	Ti_2	Na_2	$(Si_2O_7)_2O_4$	$(H_2O)_2$	$(Ca\square)(H_2O)_5$	5.387	7.091	15.473	96.580	93.948	89.818	$P\bar{1}$	1	(2)
schüllerite*** B6(GIV)		Ti_2	Mg_2	Na_2	$(Si_2O_7)_2O_2F_2$		Ba_2	5.396	7.071	10.226	99.73	99.55	90.09	$P\bar{1}$	1	(3)
lomonosovite B2(GIV)	Na_2	Ti_2	Ti_2	Na_2	$(Si_2O_7)_2O_4$		$Na_6(PO_4)_2$	5.4170	7.1190	14.4869	99.957	96.711	90.360	$P\bar{1}$	1	(1)
betalomonosovite B8(GIV)	Na_2	Ti_2	Ti_2	$^{[5]}Na_2$	$(Si_2O_7)_2O_2(OF)$		$Na_2\square_4[PO_3(OH)]$ $[PO_2(OH)_2]$	5.3331	14.172	14.509	103.174	96.320	90.278	$P\bar{1}$	2	(4)
quadruphite B3(GIV)	Na_2	Ti_2	Ti_2	Na_2	$(Si_2O_7)_2O_4$		$Na_8Ca_2(PO_4)_4F_2$	5.4206	7.0846	20.3641	86.89	94.42	89.94	$P1$	1	(5)
sobolevite B4(GIV)	Na_2	Ti_2	(TiMn)	Na_2	$(Si_2O_7)_2O_2(OF)$		Na_9Ca_2Mn $(PO_4)_4F_2$	7.0755	5.4106	40.623		93.156		Pc	2	(6)
polyphite B5(GIV)	Na_2	Ti_2	Ti_2	Na_2	$(Si_2O_7)_2O_4$		$Na_{14}Ca_4Mn$ $(PO_4)_6F_4$	5.3933	7.0553	26.451	95.216	93.490	90.101	$P\bar{1}$	1	(6)

*The ideal structural formulae are presented as the sum of the titanium-silicate (TS) block, $A^{P}_2M^{H}_2M^{O}_4(Si_2O_7)_2X^{O}_4X^{P}_4$, and the intermediate (**I**) block, in accord with Sokolova (2006); A^{P} = cations at the peripheral (*P*) sites; M^{H} = cations of the H sheet; M^{O} = cations of the O sheet; X^{O}_4 = anions shared between O and H sheets and not bonded to Si atoms; X^{P}_4 = apical anions of the M^{H} and A^{P} cations (where X^{P} anions are ligands of P^{5+} cations they are considered as part of the **I** block); coordination numbers are given for non-octahedral sites in the TS block;

**In accord with Sokolova & Cámara (2013), Bn(GIV) denotes B for basic structure of group IV, n = 1–8;

***Ba and Ca atoms occur at the A^{P} site which is shifted from the plane of the H sheet; hence we consider Ba_2 and (Ca□) as the **I** block.

References (the most recent reference on the structure): (1) Cámara *et al.* (2008); (2) Cámara *et al.* (2013); (3) Sokolova *et al.* (2013); (4) this work; (5) Sokolova & Hawthorne (2001); (6) Sokolova *et al.* (2005).

a composition based on the chemical analysis of Semenov *et al.* (1961); they gave its ideal chemical formula as $Na_2Ti_2Si_2O_9{\cdot}NaPO_3 = Na_2Ti_2Si_2O_8{\cdot}NaPO_4$. Note that the crystal structure of betalomonosovite was not yet known. The crystal structure of betalomonosovite from the Khibiny alkaline massif was determined by Rastsvetaeva *et al.* (1975) (Table 2). They reported Na disorder at several *Na* sites and the presence of both $PO_3(OH)$ and $PO_2(OH)_2$ groups. Rastsvetaeva *et al.* (1975) wrote the chemical and the detailed crystal-chemical formulae as follows: $Na_7Ti_4Si_4P_2O_{23}(OH)_3$ and $Na_2Ti_2[Na_2Ti_2Si_4]O_{18}Na_3[PO_3(OH)][PO_2(OH)_2]$, $Z = 2$. Rastsvetaeva (1986) refined the crystal structure of betalomonosovite from the Lovozero alkaline massif, confirmed the structure model of Rastsvetaeva *et al.* (1975), but reported the presence of only $PO_2(OH)_2$ groups in the betalomonosovite structure (Table 2). Rastsvetaeva (1988) and Khalilov (1990) refined the crystal structure of betalomonosovite from the Lovozero alkaline massif from the same sample, 1867/2 of A.P. Khomyakov (Table 2), using the same set of experimental X-ray single-crystal data collected by A.D. Khalilov prior to 1988. Rastsvetaeva (1988) called the 1867/2-sample of betalomonosovite the *disordered variety* of betalomonosovite. Rastsvetaeva (1988) and Khalilov (1990) reported the presence of $PO_2(OH)_2$ tetrahedra and Na disorder at several *Na* sites. The crystal-chemical formula of betalomonosovite (Rastsvetaeva 1988) and the ideal chemical formula of betalomonosovite (Khalilov 1990) (excess charge 2+) are given in Table 2. Rastsvetaeva (1989) revised the structure work of Rastsvetaeva *et al.* (1975) and Rastsvetaeva (1986, 1988), introduced three varieties of betalomonosovite characterized by different degrees of disorder at the cation sites, and discussed a domain structure for betalomonosovite based on orientations of the P tetrahedra. Despite the several structure refinements of betalomonosovite, there is no direct proof for the presence of $PO_2(OH)_2$ groups. Note that Rastsvetaeva *et al.* (1975) reported the presence of $PO_3(OH)$ and $PO_2(OH)_2$ groups in the crystal structure of betalomonosovite, which is at variance with bond-valence sums for some O atoms of the assigned OH groups and the P–OH distances. Consider O(21), an O atom of an assigned OH group of the $PO_3(OH)$ tetrahedron (Rastsvetaeva *et al.* 1975): the bond-length P–O(21) = 1.49 Å, and the sum of bond-valence contributions from P and Ti to O(21) is 1.78 *vu* (*vu* = valence units; bond-valence parameters are from Brown 1981). This bond-valence calculation ignores an additional contribution from the Na(6) atom, and we conclude that O(21) cannot be an O atom of an OH group. Similar problems arise in later refinements of betalomonosovite. Until now, there has been no spectroscopic evidence for the presence of H_2O or OH groups in the structure of betalomonosovite.

TABLE 2. STRUCTURAL STUDIES OF BETALOMONOSOVITE

Sample #	Sample provenance*	*a* (Å) α (°)	*b* (Å) β (°)	*c* (Å) γ (°)	Sp.gr. *Z*	Structural formula** O sheet	2H sheets	**I** block	Ref.
1	Khibiny	5.34	14.26	14.229	$P\bar{1}$	$Na_2Ti_2O_4$	$[Na_2Ti_2Si_4]O_{14}$	$Na_3[PO_3(OH)][PO_2(OH)_2]$	(1)
		102.55	105.87	89.10	2				
2***	Lovozero	5.326	14.184	14.47	$P\bar{1}$	$[Na_{1.1}(Ti_{1.7}Fe^{3+}_{0.3})O_4]$	$[(Ti_{1.3}Nb_{0.3}Zr_{0.15}\ Mn^{2+}_{0.2}Mg_{0.05})(Na_{1.2}Ca_{0.1}K_{0.2})(Si_2O_7)_2]$	$[Na_{2.6}(H_2PO_4)_2]$	(2)
		102.2	95.5	90.17	2				
3	Lovozero	5.351	7.131	14.488	$P1$	$\{Na_{1.22}[(Ti_{1.6}Fe^{3+}_{0.4})O_4]\}$	$\{Na_{1.28}[(Ti_{0.8}Nb_{0.2})(Ti_{0.4}Nb_{0.2}Mn_{0.15}Fe^{3+}_{0.25})(Si_2O_7)_2]\}$	$\{(Na_{3.05}Ca_{0.5})[PO_2(OH)_2]_2\}$	(3)
1687/2†	Mt. Pyalkimporr	102.1	95.24	90.2	1				
3	Lovozero	5.351	7.131	14.488	$P1$	$Na_2Ti_2O_2(OH,F)_2$	$[NaTiSi_2O_7]_2$	$Na_2[PO_2(OH)_2]_2$	(4)
1687/2†	Mt. Pyalkimporr	102.1	95.24	90.2	1				

*Sample provenance is Kola Peninsula, Russia: first line gives the name of the alkaline massif; second line, of the mountain;
**Ideal structural formula is given in (1) and (4);
***Unit cells for samples 1 and 2 are related: $\mathbf{a}_2 = -\mathbf{a}_1$; $\mathbf{b}_2 = \mathbf{b}_1$; $\mathbf{c}_2 = \mathbf{a}_1 + \mathbf{c}_1$;
† Sample of Khomyakov (1990): structure refinements reported in (3) and (4) were done using the single-crystal X-ray data from the same crystal of betalomonosovite.
References: (1) Rastsvetaeva *et al.* (1975); (2) Rastsvetaeva (1986); (3) Rastsvetaeva (1988); (4) Khalilov (1990).

Description of Samples of Betalomonosovite and Lomonosovite

A pale-brown single crystal of betalomonosovite, a small thin plate (0.160 × 0.120 × 0.025 mm), was selected from sample 1867/2 of A.P. Khomyakov for the collection of X-ray diffraction data. Two additional grains of betalomonosovite were selected from the same sample (1867/2) for microprobe analysis, and a few more grains for infrared and Raman spectroscopy. The crystals of betalomonosovite used in this work are from Pyalkimporr Mountain, Lovozero alkaline massif.

For the infrared spectroscopy, we used crystals of the holotype lomonosovite sample 42704 from the Lovozero tundra, Kola Peninsula, Russia (Fersman Mineralogical Museum, Moscow, Russia) and for high-resolution transmission electron microscopy (HRTEM) we used crystals of lomonosovite from the Khibiny alkaline massif, Kola Peninsula, Russia (Royal Ontario Museum, Toronto, Canada; sample M36448).

Fourier-Transform Infra-red Spectroscopy (FTIR)

Experimental details

Powder (standard KBr pellet) FTIR spectra for betalomonosovite and lomonosovite were collected using a Bruker Tensor 27 FTIR spectrometer equipped with a KBr beam splitter and a DLATGS detector. For single-crystal FTIR, a Bruker Hyperion 2000 IR microscope was used, which is equipped with a liquid-nitrogen-cooled MCT detector. Spectra over the range 4000–400 cm^{-1} (4000–650 cm^{-1} for single-crystal FTIR) were obtained by averaging 100 scans with a resolution of 4 cm^{-1}. Baseline correction was done using the OPUS spectroscopic software (Bruker Optic GmbH). Band analysis was done using the program Fityk 0.9.8 (Wojdyr 2010).

Band assignment

The FTIR spectra of lomonosovite (holotype) and betalomonosovite are shown in Figure 1. In the OH-stretch region, 4000–3000 cm^{-1}, the lomonosovite (holotype) KBr-spectrum (Fig. 1a) shows a band at ~3360 cm^{-1}, with a shoulder at ~3500 cm^{-1}, superimposed on a broad H_2O-like feature that extends down to ~2800 cm^{-1}. These bands are well defined in the single-crystal spectrum (Fig. 1b) and occur at 3365 and 3525 cm^{-1}, respectively. The 3525 cm^{-1} band may be assigned to an OH group, and the 3365 cm^{-1} band along with the broad feature is due to H_2O stretches. The peaks observed at ~1640 and 1600 cm^{-1} (a shoulder) are assigned to the H–O–H bending. The structure of lomonosovite does not contain either H_2O or OH groups (Cámara *et al.* 2008), and hence the presence of bands in the infrared spectrum attributable to H_2O and OH must be due to (1) the presence of an additional contaminating hydroxy-hydrated phase in the powder used for the collection of the spectrum, or (2) submicroscopic intergrowth of a hydroxy-hydrated phase in the crystals of lomonosovite. Bands associated with H_2O stretching and bending vibrations have also been observed in the FTIR spectrum of lomonosovite studied by Frost *et al.* (2015).

The betalomonosovite FTIR spectra in the 4000 to 2000 cm^{-1} region (Figs. 1c, d) show a broad band centered at ~3100 cm^{-1}, with a shoulder at ~3500 cm^{-1}, and a less-intense band at ~2400 cm^{-1}. The 3500 cm^{-1} band, which is relatively narrow, is assigned to (M)O–H stretches, where M is mainly Na and Ti. The 3100 and 2400 cm^{-1} bands are characteristic of the (P)O–H stretching vibrations, referred to in the literature as band A and band B, respectively (Table 3), indicating the presence of $PO_3(OH)$ and $PO_2(OH)_2$ groups in the structure (Chapman & Thirlwell 1964, Cooper *et al.* 2013). The in-plane P–O–H bending vibrations are observed in the single-crystal spectrum at 1285 and 1245 cm^{-1} (Fig. 1d). In the 1200–600 cm^{-1} region, bands at 710(shld), 800(shld), 915(str), 944(str), 1045(shp), 1090(shld), and 1150(shld) are observed in the KBr-pellet spectrum (Fig. 1c) and are mostly saturated in the single-crystal spectrum (Fig. 1d). These bands are assigned to stretching vibrations of the Si_2O_7, $PO_3(OH)$, and $PO_2(OH)_2$ groups in the structure of betalomonosovite. The weak bands between 1900 and 1500 cm^{-1} are mainly due to combinations (Band C, Table 3).

Figure 2 shows the single-crystal FTIR spectrum of betalomonosovite in the region 3730–1450 cm^{-1} with the bands deconvoluted into different Gaussian peaks. Using Table 3 and the structure-refinement results (below), we may assign these peaks as follows: the peak at 3529 cm^{-1} is assigned to (Na)O–H stretches and the two peaks at 3457 and 3295 cm^{-1} to H_2O stretches (with the H–O–H bend peaks observed at 1645 and 1581 cm^{-1}). The structure of betalomonosovite does not contain H_2O groups, and hence the presence of H_2O bands in the infrared spectrum must be due to (1) the presence of an additional contaminating hydroxy-hydrated phase in the powder used for the collection of the spectrum, or (2) submicroscopic intergrowth of a hydroxy-hydrated phase in the crystals of betalomonosovite. The strong peak at 3053 cm^{-1} and the less intense peak at 2766 cm^{-1} are assigned to the principal (P)O–H stretches (band A). Note that the B and C bands are also fitted with two components (2408 and 2305 cm^{-1}, and 2198 and 2080 cm^{-1}) for the B bands and two (1816 and 1748 cm^{-1}) for the C band (Fig. 2). The deconvolution of the principal (P)O–H stretch band (band A), and the associated bands (B) and (C), into two components

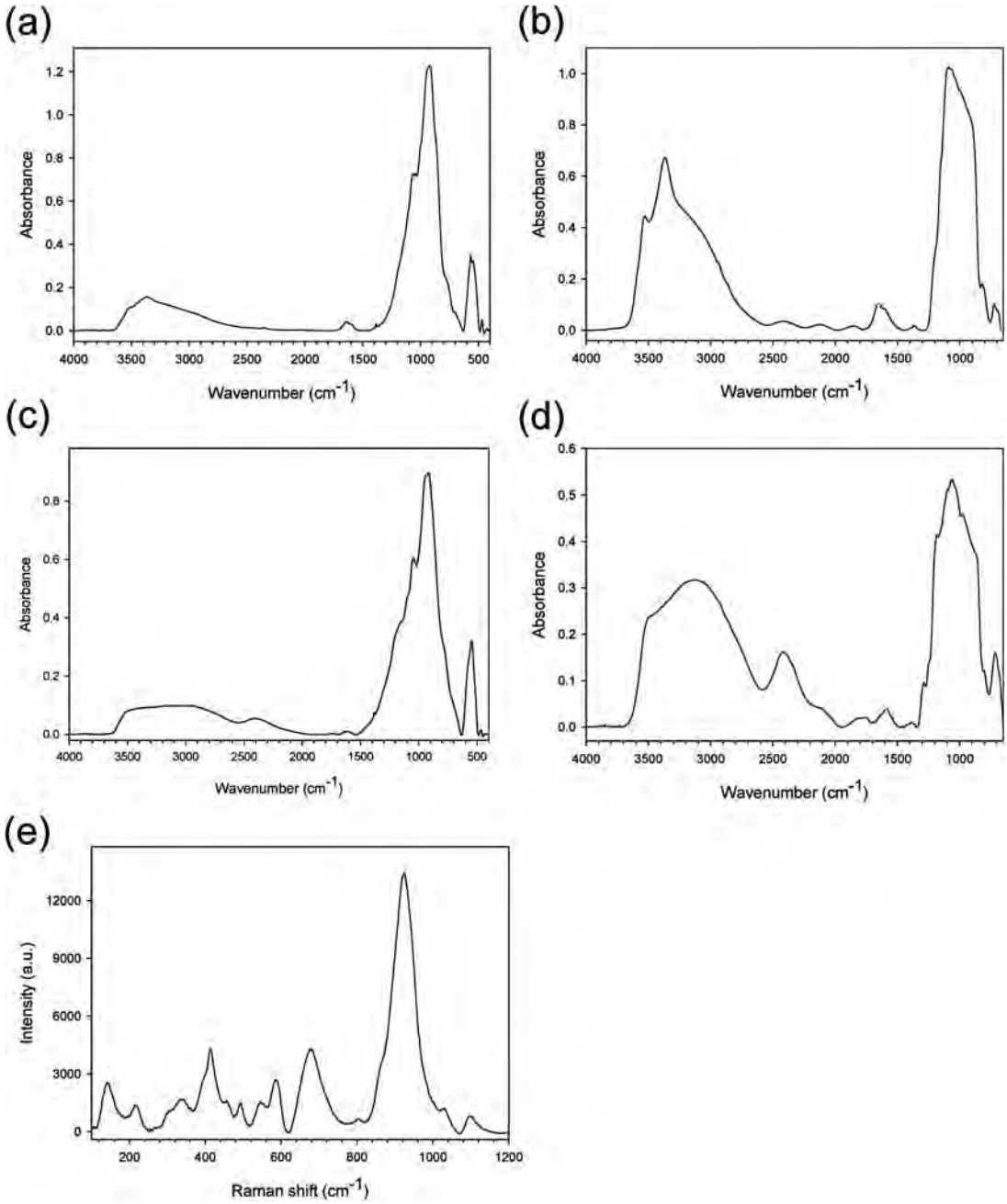

FIG. 1. FTIR spectra of lomonosovite (holotype): (a) KBr-pellet and (b) single-crystal, and betalomonosovite: (c) KBr-pellet and (d) single-crystal, and the Raman spectrum (100–1200 cm^{-1}) of betalomonosovite (e).

suggests that there are at least two symmetrically distinct $PO_3(OH)/PO_2(OH)_2$ groups at the different *P* sites (Taher *et al.* 2001, Cooper *et al.* 2013). Thus, we may assign the prominent peak at 3053 cm^{-1} to OH groups belonging to the P(1,2) tetrahedra and the peak at 2766 cm^{-1} to OH groups belonging to the P (3,4) tetrahedra; these two distinct OH groups have different hydrogen-bond strengths. Using the d(O...

TABLE 3. IR BANDS (4000–700 cm^{-1}) OF $(HPO_4)^{2-}$ AND $(H_2PO_4)^{-}$ GROUPS

Na_2HPO_4 [1]	$Na_2HPO_4(H_2O)_2$ [1]	NaH_2PO_4 [1]	α-$Ge(HPO_4)_2(H_2O)$ [2]	$CdBa_2(HPO_4)_2(H_2PO_4)_2$ [3]	Assignment
	3350 s, 3050 s		3547, 3460		H_2O stretch
2820 s, br	2870 m	2780 s, br	2940	2750 s, br	(P)O–H stretch (band A)
2400 s, br	2430 w, 2320 w	2360 s, br	2370	2460 sh, 2370 s, 2315 s, 2199 sh	(P)O–H stretch (band B) overtone of P–O modes (2)
1780 s, br	1700 w	1650 s, v.br	1622	1749 m, br	Combination mode (band C) / H_2O bend
1388 m	1256 m	1280 s	1261	1279 s, 1264 sh, 1226 m	In-plane P–O–H bend
1352 m		1240 m 1098 m			
1150 s	1135 s, 1120 s	1166 s	1190, 1130, 1100	1151 s, 1102 sh, 1073 vs	P–O stretch
1068 s	1070 s, 1055 s	1120 s	1075, 1031, 972	1044 vw, 1019 s, 994 w	
948 s	993 s, 953 s	1053 vs	956	942 s, 911 s, 892 s, 850 sh	
970 m, br	766 m	820 w	770	775 w	Out-of-plane P–O–H bend
860 s	866 s 820 s, br	989 s 932 vs 875 m			P–O(H) stretch

References: [1] Chapman & Thirlwell (1964); [2] Moraes *et al.* (2006); [3] Taher *et al.* (2001).

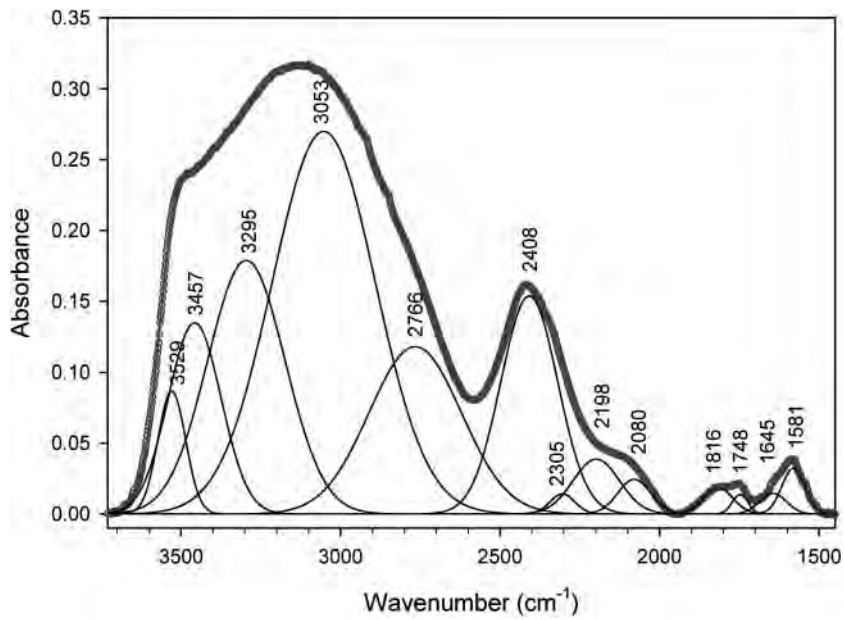

FIG. 2. Resolution of the IR bands in the 3730–1450 cm^{-1} region of the betalomonosovite single-crystal spectrum (see text for details).

O)– frequencies correlation of Libowitzky (1999), the calculated OH...O distances for the 3053 and 2766 cm^{-1} bands are 2.66 and 2.61 Å, respectively. The former value is in accord with the OH...O distance in the P(1,2) tetrahedra [2.68(1) Å] calculated from the structure refinement (as discussed below).

Raman Spectroscopy

Experimental details

The Raman spectrum of betalomonosovite in the range 100–4000 cm^{-1} was collected in back-scattered geometry using a HORIBA Jobin Yvon-LabRAM ARAMIS integrated confocal micro-Raman system equipped with a 460 mm focal length spectrograph and a multichannel air-cooled (–70 °C) CCD detector. A 100× objective lens was used with an estimated spot size of ~1 μm, a 1800 gr/mm grating, and a 532 nm excitation laser. The wavenumber was calibrated using the 520.7 cm^{-1} line of Si metal. Baseline correction was done using the LabSpec5 software package.

Band assignment

The Raman spectrum of betalomonosovite in the region 100–1200 cm^{-1} is shown in Figure 1e. No Raman peaks were observed in the 1200 to 4000 cm^{-1} region. The bands in the region 800–1200 cm^{-1}, with a prominent peak at 925 cm^{-1} and weak peaks/shoulders at 804, 862, 1030, and 1100 cm^{-1}, are assigned to the stretching vibrations of the Si_2O_7 and $PO_3(OH)$ groups. The shoulder at 862 cm^{-1} may be assigned to the P–OH stretch of the $PO_3(OH)$ group. However, the symmetric stretching mode of SiO_3 of the Si_2O_7 group also gives rise to a peak at ~860 cm^{-1} (Le Cléac'h & Gillet 1990). The band at 678 cm^{-1} is assigned to the stretching vibrations of the Si–O–Si bridges of the Si_2O_7 group (Le Cléac'h & Gillet 1990). The peaks at 587, 548, 493, 456, and 414 cm^{-1} may be assigned to the bending vibrations of the Si_2O_7, $PO_3(OH)$, and $PO_2(OH)_2$ groups, and those below 400 cm^{-1} to the lattice modes.

Transmission Electron Microscopy (TEM)

Experimental details

The TEM samples were prepared by enclosing single crystals of betalomonosovite and lomonosovite, previously oriented via single-crystal X-ray diffraction, between graphite bricks with epoxy resin so as to have the **c**-axis nearly perpendicular to the bricks. TEM cross-sections were prepared from these "sandwiches" *via* mechanical polishing and subsequent ion milling. High-resolution TEM (HRTEM) observations, high-angle annular dark field (HAADF) imaging done in scanning TEM (STEM) mode, and selected-area electron-diffraction (SAED) patterns were acquired with a JEOL JEM 2200FS microscope equipped with a Schottky field emission gun working under an acceleration voltage of 200 kV, a CEOS spherical-aberration corrector of the objective lens allowing a spatial resolution of 0.9 Å, and an in-column energy Omega filter. All HRTEM data were acquired using an energy slit 20 eV wide in order to filter only zero-loss Bragg-scattered signals and eliminate the inelastic scattering. Energy Dispersive X-ray Spectroscopy (EDX) analysis was done in STEM mode using a Bruker XFlash Silicon Drift Detector with an active area of 60 mm^2 and a JEOL double-tilt TEM holder equipped with a low-background beryllium tip. Chemical STEM-EDX characterization was done using an electron probe 1 nm wide in order to achieve good spatial resolution with high signal/noise ratio.

Discussion

The samples of betalomonosovite and lomonosovite underwent moderate electron beam damage in the TEM experiment. Therefore the crystal sections were coated with a carbon film 5 nm thick to reduce electron beam-damage and electrostatic charge effects.

TEM survey observations of both phases show pervasive defective structures characterized by a ubiquitous structurally related band texture. This texture consists of defective {001} lamellae with different thickness (from 10 to 100 nm) interleaved with defect-free bands and alternating along the [001] direction (Genovese *et al.* 2014).

Figure 3a presents a typical HRTEM image of betalomonosovite observed along the [010] zone axis and showing the {001} lamellar texture. Defect-bearing and defect-free lamellae are separated by semicoherent {001} interfaces. The microstructure of undisturbed regions consists of a regular repetition of unit cells which exhibit the main {100} and {001} lattice planes with projected unit-cell vectors of 5.3 Å and 14.1 Å, respectively, and forming an angle of 96.3°. The [010] Fast Fourier Transform (FFT) patterns, extracted from the HRTEM data, are compatible with the SAED pattern of the reciprocal a*c* plane. The projected crystal potential within defect-bearing regions displays a pale and faint contrast, as shown in the central lamella in Figure 3a. Along this lamella, the crystal structure periodicity is not evident and only rare and wavy {00l} planes can be identified. This feature could be ascribed to a marked loss of crystallinity in those areas of the crystal where the defect density is greater and associated with an important variation in the chemical composition. STEM-EDX chemical analysis (Fig. 3b) displays a variation of cation/anion distribution; in particular, defect-bearing lamellae, characterized by darker

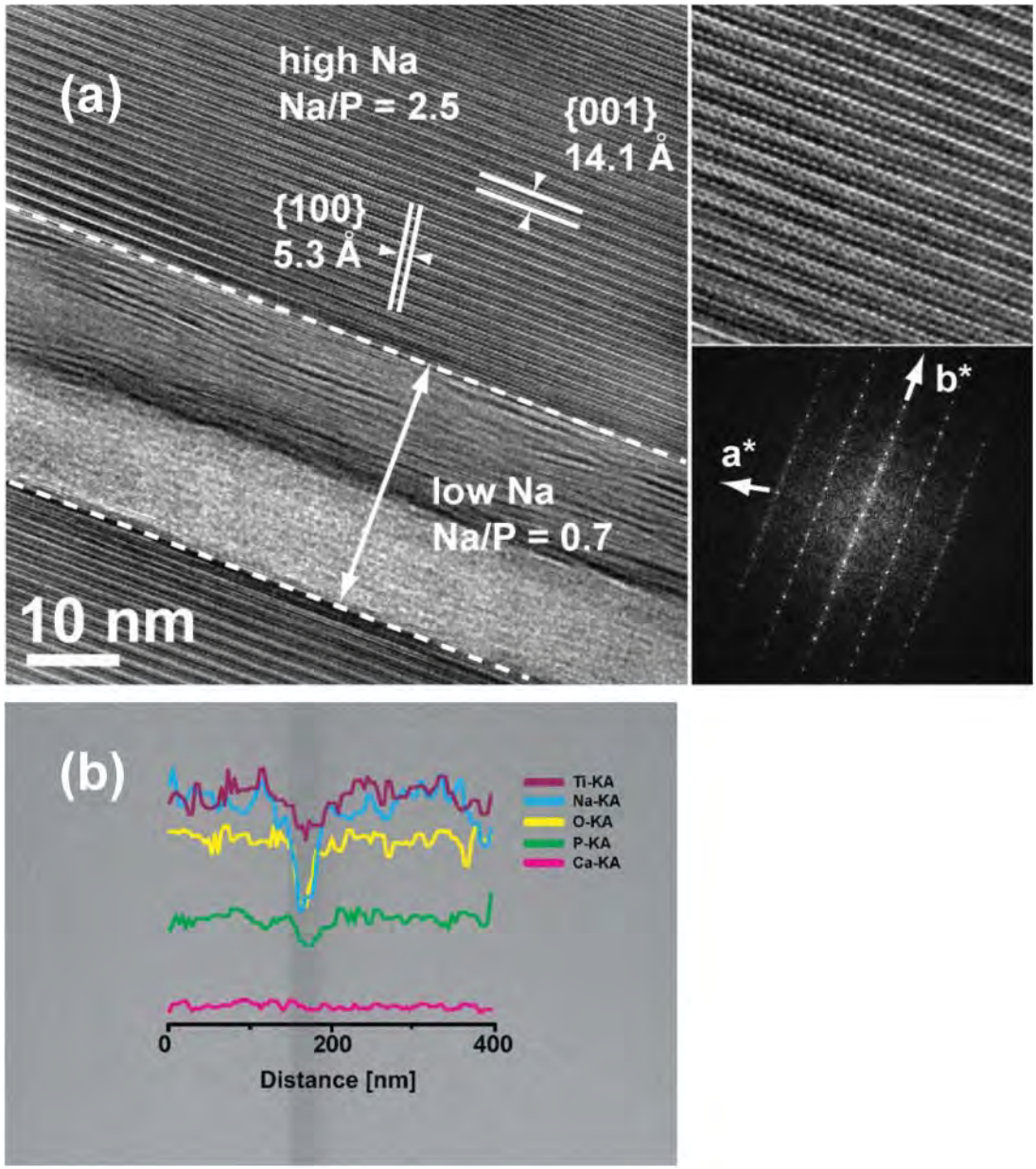

FIG. 3. TEM characterization of betalomonosovite. (a) [010] HRTEM projection of band structure showing interleaved lamellae separated by semicoherent interfaces, characterized by a variation of Na/P atom ratio and different projected crystal potential. In the upper and lower regions the projected crystal structure exhibits {001} and {100} lattice planes with *d*-spacings of 14.1 and 5.3 Å, respectively; it is notable that there is poor crystallinity in the intermediate lamella where {00l} defect-rich ribbons are recognizable. The panels on the right show details of a defect-free area showing the fine structure and the corresponding FFT pattern consistent with the a*c* SAED pattern; (b) STEM-EDX line mapping (black profile) reports the elements distribution across the lamellae showing a decrease of Na, O, Ti, and P in the central band (darker HAADF contrast) and a constant Ca distribution.

contrast in HAADF STEM imaging, exhibit a Na/P atom ratio less than 1 and a lower content of Na, O, Ti, and P if compared to the content of Na, O, Ti, and P in defect-free bands with a Na/P atom ratio greater than 2; it should be noted that no significant variation in Ca distribution is present.

Lomonosovite also has a similar lamellar microstructure, with {001} lamellae interleaved along the [001] direction and connected by semicoherent interfaces (Fig. 4a). A typical [100] HRTEM projection of defect-free regions shows undisturbed repetition of the unit-cell vectors along [010] and [001] and exhibits the main {010} and {001} lattice planes with *d*-spacings of 7.0 and 14.2 Å, respectively, forming an angle of 100°. Conversely, defect-bearing bands are characterized by a partial loss of structural

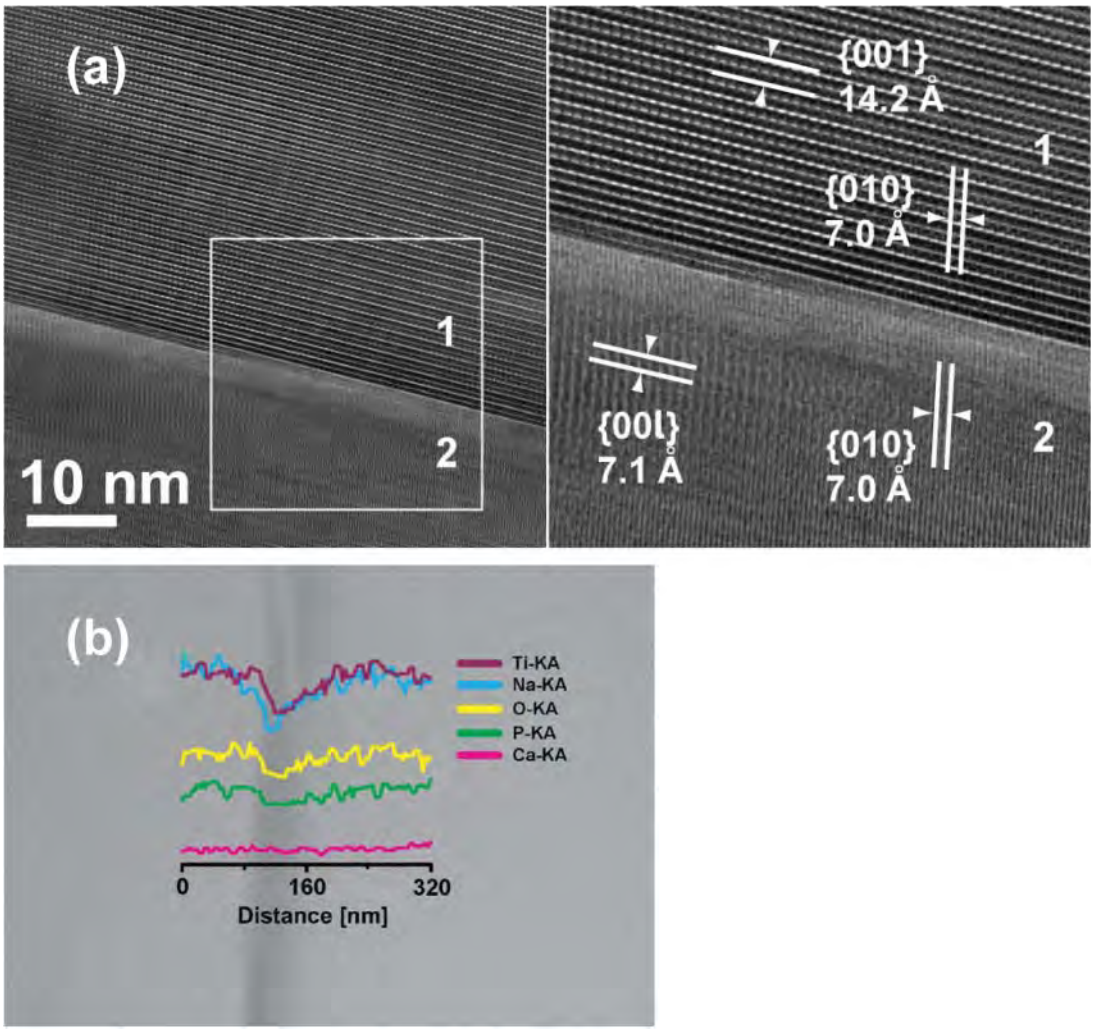

FIG. 4. TEM characterization of lomonosovite. (a) [100] HRTEM projection of a typical defect-bearing region showing two main lamellae characterized by different projected crystal potential and separated by semicoherent contact interfaces. The panel on the right displays details (with square) of the projected structure: lamella (1) clearly shows undisturbed crystal structure with continuous periodicity along [001] and [010] directions and exhibiting {001} and {010} lattice planes with *d*-spacing of 14.2 and 7.0 Å, respectively; lamella (2) is characterized by a partial loss of crystal periodicity along the [001] direction, only {010} lattice planes are distinctly preserved, conversely blurred {00l} lattice planes with *d*-spacing of about 7.1 Å can hardly be recognized; (b) STEM-EDX line profile (black line) shows elements distribution across the lamellae, exhibiting a decrease of Ti, Na, O, and P in the central lamella (darker contrast) that corresponds to the defect-bearing ribbons and no Ca variation.

periodicity along the [001] direction, displaying blurred and fragmented {00l} lattice planes with a *d*-spacing of about 7.1 Å, which might be indexed as {002}. However, the structural periodicity is retained along [010], showing sharp {010} lattice planes. It is notable that the {010} lattice planes are continuous through the interfaces between the lamellae (see right panel of Fig. 4a). The loss of [001] periodicity may be related to both the variation of chemical composition of defect-bearing lamellae and the presence of the same structural defects, as is shown by STEM-EDX analysis (Fig. 4b). These lamellae, with darker contrast in HAADF STEM imaging, show a lower content of Ti, Na, O, and P and no significant changes in Ca distribution, as in betalomonosovite.

Electron-Microprobe Analysis

The two grains of betalomonosovite used here have a platy habit; one grain (0.942 × 0.320 × 0.030 mm) was polished and the other grain (0.814 × 0.257 × 0.025 mm) was not. Both grains were analyzed with a Cameca SX-100 electron-microprobe operating in wavelength-dispersion mode with an accelerating voltage of 15 kV, a specimen current of 15 nA, a beam size of 15 μm, and count times on peak and background of 20 and 10 s, respectively. The following standards were used for *K*α or *L*α X-ray lines (analyzing crystals are given in brackets): F(TAP): F-bearing riebeckite; Na(TAP): albite; Ca(PET): diopside; Nb(PET): $Ba_2NaNb_5O_{15}$; P(PET): apatite; Si(TAP), Ti(LiF): titanite; Ta(LiF): $Mn(Ta_{1.7}Nb_{0.3})O_6$; Mn(LiF): spessartine; Mg(TAP): forsterite; Fe(LiF): fayalite; Zr(PET): zircon. Data were reduced using the φ(ρZ) procedure of Pouchou & Pichoir (1985). In order to account for Na migration under the electron beam, Na was analyzed first with crystal TAP, and a linear-decay model was obtained from counts at different times, which was then used to correct the Na counts. The chemical composition of betalomonosovite is given in Table 4 and is the mean of 10 determinations. The empirical formula for betalomonosovite (Table 4) was calculated on the basis of 26 (O + F) anions: $(Na_{5.39}Ca_{0.36}Mn_{0.04}Mg_{0.01})_{\Sigma 5.80}(Ti_{2.77}Nb_{0.48}Mg_{0.29}Fe^{3+}_{0.23}Mn_{0.20}Zr_{0.02}Ta_{0.01})_{\Sigma 4}(Si_{2.06}O_7)_2[P_{1.98}O_5(OH)_3]O_2[O_{0.82}F_{0.65}(OH)_{0.53}]_{\Sigma 2}$, $D_{calc.}$= 2.969 g cm^{-3}, Z = 2, with H_2O determined from structure refinement and in accord with the results of FTIR spectroscopy. Table 4 reports previous chemical analyses of betalomonosovite from the literature and the latest chemical analysis of lomonosovite. Analyses (3A), (3B), and (5) (this work) were done using the same sample (1867/2 of A.P. Khomyakov) and they show good agreement. There is also good agreement between $D_{calc.}$ = 2.969 g cm^{-3} (this work) and $D_{meas.}$ = 2.98 g cm^{-3} (Gerasimovskiy & Kazakova 1962).

Crystal Structure: Experimental Details

Data collection and structure refinement

Single-crystal X-ray diffraction data for betalomonosovite were collected with a APEX II ULTRA three-circle diffractometer with a rotating-anode generator (Mo*K*α), multilayer optics, and an APEX-II 4K CCD detector. The intensities of 12453 reflections with $\bar{7} \le h \le 7$, $\bar{20} \le k \le 20$, $\bar{20} \le l \le 20$ were collected with a frame width of 0.3° and a frame time of 2 s, out to 2θ = 60.4°. The refined unit-cell parameters were obtained from 9055 reflections ($I > 10\sigma I$) and are given in Table 5. The doubled b = 14.172 Å is supported by the presence of weak reflections ($I < 10\sigma I$) along **b** and is in good agreement with the unit-cell parameters of Rastsvetaeva *et al.* (1975) and Rastsvetaeva (1986) (Table 2). An empirical absorption correction (SADABS, Sheldrick 2008) was applied. The Bruker SHELXTL Version 5.1 system of programs (Sheldrick 2008) was used for refinement of the betalomonosovite structure. The crystal structure of betalomonosovite was refined in space group $P\bar{1}$ with initial atom coordinates of Rastsvetaeva (1986): Ti(1–4), Si(1–4), P(1–3), Na(1–10), and O(1–28). During the refinement, five additional atoms, P(4) and O(29–32), (at partly occupied sites) were located in the difference-Fourier map and included in the refinement. The occupancies of the Ti-dominant, Na-dominant, and Ca-dominant sites were refined with the scattering curves of Ti, Na, and Ca, respectively. Note that the Na-dominant, Ca-dominant, and P-dominant sites also include sites where vacancy (□) is a dominant species, *e.g.*, (□,Na) [*Na*(7,8)]; (□,Ca) [*A*(1,2)]; and (□,P) [*P*(3,4)]. Neutral scattering curves were used for O and Si atoms. Scattering factors were taken from the International Tables for X-ray Crystallography (1992).

There is extensive cation and anion disorder in the crystal structure of betalomonosovite. Of ten alkali-cation sites, only two sites are fully occupied by Na, four sites are more than 50% occupied by Na, and four sites are occupied to 22–14% by Na and Ca [*Na*(7,8); *A*(1,2)]. The *Na*(3) and *A*(1) sites and *Na*(4) and *A*(2) sites occur at short distances of 2.25 and 2.16 Å, respectively. Two *P* sites split into two subsites each, with 86% [*P*(1,2)] and 14% [*P*(3,4)] occupancies and separated by short distances: P(1)–P(3) = 0.67 and P(2)–P(4) = 0.60 Å. The occupancies of the *Ti, P*, *Na*, and *A* sites were refined, adjusted in accord with chemical analysis, and then fixed. Occupancies of the O atoms tetrahedrally coordinating P(1,2) (86%-occupancy) and P(3,4) (14%-occupancy) atoms were refined in isotropic approximation and fixed in accord with the site-occupancy of the central cation: 86% for O(21–26) and 14% for O(27–32). There were very few reflections at high θ, and for the last stages of the refinement, the X-ray diffraction data

TABLE 4. CHEMICAL ANALYSIS (wt.%) AND FORMULA UNIT (*apfu*) FOR BETALOMONOSOVITE

Oxide	Betalomonosovite								Lomonosovite
	(1A)	(1B)	(2)	(3A)	(3B)	(4A)	(4B)	(5)	(6)
Nb_2O_5	3.05*	4.78*	4.00	5.41	5.40	0.94	1.04	6.75	6.50
Ta_2O_5			0.52	n.a.	n.a.	n.a.	n.a.	0.14	0.21
P_2O_5	18.54	16.12	15.05	14.58	14.40	13.43	15.12	14.85	13.37
ZrO_2	2.24	1.89	2.50	n.d.	0.40	n.a.	n.a.	0.20	1.28
TiO_2	23.85	25.01	25.66	23.73	23.10	29.22	26.64	23.46	21.67
SiO_2	24.60	25.18	24.81	25.30	24.80	26.52	26.57	26.25	23.28
Al_2O_3	n.a.	0.69	0.40	n.a.	n.a.	n.d.	n.d.	n.d.	n.d.
Fe_2O_3	2.13	2.38	2.20	1.82	0.00	2.82	2.74	1.97	0.46
FeO	0.00	0.00	0.00	0.00	1.90	0.00	0.00	0.00	0.69
BaO	n.a.	n.a.	n.a.	n.a.	2.00	n.a.	n.a.	n.d.	n.d.
SrO	n.a.	n.a.	n.a.	n.a.	0.30	n.a.	n.a.	n.d.	n.d.
MnO	0.96	1.40	1.70	1.28	1.80	0.46	0.94	1.80	2.91
CaO	1.66	0.62	1.80	3.00	2.90	2.88	2.59	2.12	0.57
MgO	0.24	0.22	0.30	n.d.	1.10	0.35	0.73	1.26	0.44
K_2O	n.a.	0.88	0.90	0.95	n.d.	0.37	0.17	n.d.	n.d.
Na_2O	16.50	17.13	15.16	18.04	19.00	17.17	17.82	17.70	28.22
F	n.a.	n.a.	n.a.	1.02	0.60	n.a.	n.a.	1.31	0.91
H_2O	5.70	3.50	5.10	5.05	n.a.	n.a.	n.a.	3.18	n.d.
O=F	0.00	0.00	0.00	0.43	0.25	0.00	0.00	0.55	–0.38
Total	99.47	99.80	100.10	99.75	97.45	94.16	94.36	100.44	100.13
	Formula unit on the basis of 26 (O + F) *apfu*.								
Nb^{5+}	0.21**	0.34**	0.28	0.38	0.43	0.07	0.08	0.48	0.51
Ta^{5+}			0.02	0.00	0.02	0.00	0.00	0.01	0.00
P^{5+}	2.40	2.16	1.99	1.93	2.11	1.96	2.20	1.98	1.96
Zr^{4+}	0.17	0.15	0.19	0.00	0.03	0.00	0.00	0.02	0.11
Ti^{4+}	2.74	2.98	3.01	2.79	3.02	3.80	3.44	2.78	2.83
Si^{4+}	3.76	3.99	3.87	3.96	4.31	4.58	4.56	4.14	4.04
Al^{3+}	0.00	0.13	0.07	0.00	0.00	0.00	0.00	0.00	0.00
Fe^{3+}	0.25	0.28	0.26	0.21	0.00	0.37	0.35	0.23	0.06
Fe^{2+}	0.00	0.00	0.00	0.00	0.28	0.00	0.00	0.00	0.10
Ba^{2+}	0.00	0.00	0.00	0.00	0.14	0.00	0.00	0.00	0.00
Sr^{2+}	0.00	0.00	0.00	0.00	0.03	0.00	0.00	0.00	0.00
Mn^{2+}	0.12	0.19	0.23	0.17	0.27	0.07	0.14	0.24	0.43
Ca^{2+}	0.27	0.11	0.30	0.50	0.54	0.53	0.48	0.36	0.11
Mg^{2+}	0.06	0.05	0.07	0.00	0.29	0.09	0.19	0.30	0.11
K^+	0.00	0.18	0.18	0.19	0.00	0.08	0.04	0.00	0.00
Na^+	4.88	5.26	4.59	5.47	6.41	5.75	5.93	5.41	9.50
F^-	0.00	0.00	0.00	0.51	0.33	0.00	0.00	0.65	0.50
H^+	5.81	3.70	5.31	5.27	0.00	0.00	0.00	3.35	0.00
O^{2-}	26.00	26.00	26.00	25.50	25.67	26.00	26.00	25.35	25.50
CATSUM	14.85	15.80	15.05	15.60	17.87	17.30	17.39	15.95	19.76

(1) Gerasimovskiy & Kazakova (1962): wet chemistry; (1A) $H_2O^+ + H_2O^- = H_2O$ = 5.70 wt.%; analyst T.A. Burova, 1939; (1B) H_2O^+ = 3.50 wt.%, H_2O^- = 0.16 wt.%; analyst M.Ye. Kazakova, 1960; H_2O^+ = 3.50 wt.% has been used to calculate the formula; (2) Semenov *et al.* (1961): wet chemistry, $H_2O^+ + H_2O^- = H_2O$ = 5.10 wt.%; analyst M.V. Kucharchik; (3) Khomyakov (1990): EMPA; (3A) analyst A.V. Bykova; (3B) analyst G.N. Nechelyustov; (4A, 4B) Ageeva (1999): EMPA; analyst O.A. Ageeva; (5) This work: EMPA; SrO, BaO, Al_2O_3, and K_2O were sought but not detected; analyst R. Sidhu; (6) Cámara *et al.* (2008): EMPA; analyst R. Sidhu.

* $Nb_2O_5 + Ta_2O_5$; ** Nb + Ta.

Localities: Lovozero (1, 2, 3, 5, 6) and Khibiny (4) alkaline massifs, Kola Peninsula, Russia; samples (1–3, 5) and (4) of betalomonosovite are from pegmatites and feldspar-rich alkaline rocks, respectively.

TABLE 5. MISCELLANEOUS REFINEMENT DATA FOR BETALOMONOSOVITE

a (Å)	5.3331(7)
b	14.172(2)
c	14.509(2)
α (°)	103.174(2)
β	96.320(2)
γ	90.278(2)
V (Å^3)	1060.7(4)
Space group	$P\bar{1}$
Z	1
Absorption coefficient (mm^{-1})	2.33
F(000)	924.8
$D_{calc.}$ (g/cm^3)	2.969
Crystal size (mm)	0.160 × 0.120 × 0.025
Radiation/monochromator	Mo-*K*α/graphite
$2\theta_{max}$ for structure refinement (°)	50.00
R(int) (%)	1.50
Reflections collected	12453
Independent reflections	3733
$F_o > 4\sigma F$	3379
Refinement method	Full-matrix least squares on F^2, fixed weights proportional to $1/\sigma F_o^2$
No. of refined parameters	466
Final $R_{(obs)}$ (%)	
[$F_o > 4\sigma F$]	6.64
R_1	6.95
wR_2	15.13
Highest peak, deepest hole (e Å^{-3})	+1.31, –1.06
Goodness of fit on F^2	1.096

was reduced to 2θ = 50.0°. The structure refinement converged to R_1 = 6.64% and a GoF of 1.096. Details of the X-ray data collection and structure refinement are given in Table 5. Final atom parameters are given in Table 6, selected interatomic distances and angles in Table 7, refined site-scattering values and assigned populations for selected sites in Table 8, and bond-valence values in Table 9. A table of structure factors and a CIF may be obtained from The Depository of Unpublished Data on the MAC website [document betalomonosovite CM53-3 10.3749/canmin.1400044].

Site-population assignment

Here we divide the cation sites (Table 8) into four groups: (1) *Ti*(1,2) and *Na*(1,2) constitute the M^O sites of the O sheet; (2) *Ti*(3,4) (= M^H) and *Si* sites of the H sheet; (3) *Na*(3,4) (= peripheral A^P sites); and (4) *Na* (5–8), *A*(1,2), and *P*(1–4) sites of the **I** block; site labeling (M^O, M^H, A^P) is in accord with Sokolova (2006). Consider first the Ti-dominant sites. We assign cations to these sites based on our knowledge from previous work on TS-block minerals: Ti-dominant sites are always fully occupied, and Ti-dominant sites in the O sheet can have a significant content of Mn, Mg, and Fe^{2+}, as in lomonosovite (Cámara *et al.* 2008) and sobolevite, $Na_{12}Ca(NaCaMn)Ti_2(TiMn)(Si_2O_7)_2(PO_4)_4O_3F_3$ (Sokolova *et al.* 2005). Table 8 shows that the refined scattering at all *Ti*(1–4) sites is approximately the same, 23.8 *epfu*, total 23.8 × 4 = 95.2 *epfu* (electrons per formula unit). Chemical analysis gives possible cations to be assigned as follows: $(Ti_{2.77}Nb_{0.48}Mg_{0.30}Fe^{3+}_{0.23}Mn_{0.24}Zr_{0.02}Ta_{0.01})_{\Sigma 4.05}$, with a calculated aggregate site-scattering of 97.73 *epfu*. Hence we will assign 4 *apfu*: 2.77 Ti + 0.48 Nb + 0.29 Mg + 0.23 Fe^{3+} + 0.20 Mn + 0.02 Zr + 0.01 Ta, site-scattering of 96.61 *epfu*, to the *Ti*(1–4) sites; we allocate $Mg_{0.01}Mn_{0.04}$ to the alkali-cation sites. The distances <Ti(1,2)–O> = 2.017 and 2.014 Å in the O sheet are longer than <Ti(3,4)–O> = 1.960 and 1.958 Å of the H sheet. In accord with our knowledge of the *Ti* sites in the O sheet (see above), we assign 0.20 Mn and 0.29 Mg *apfu* [r = 0.83 and 0.72 Å, Shannon (1976)] to the *Ti*(1,2) sites: 1.24 Ti + 0.29 Mg + 0.24 Nb + 0.20 Mn + 0.02 Zr + 0.01 Ta, with a calculated site-scattering of 47.13 *epfu*. We assign Ti, Nb, and Fe^{3+} to the *Ti*(3,4) sites, with a calculated site-scattering of 49.48 *epfu*. The total site-scattering value of 96.61 *epfu* [*Ti*(1–4) sites] agrees closely with the refined site-scattering of 95.2 *epfu*.

Alkali-cation sites. In the betalomonosovite structure, there are 10 alkali-cation sites and each site contributes 1 *apfu*. These 10 sites correspond to the five alkali-cation sites in lomonosovite (Cámara *et al.* 2008), where each site gives 2 *apfu*. Table 4 gives the alkali cations plus minor M^{2+} cations as follows: 5.39 Na + 0.36 Ca + 0.04 Mn + 0.01 Mg = 5.80 *apfu*. This value tells us that there are not enough alkali cations to fill these 10 sites, *i.e.*, about 40% of the 10 sites must be vacant. The refined site-scattering values for the 10 alkali sites (0.8–11.0 *epfu*) (Table 8) agree with the Na disorder in the betalomonosovite structure reported by Rastsvetaeva *et al.* (1975), Rastsvetaeva (1986, 1988), and Khalilov (1990). The 5.80 *apfu* from EMPA give a total scattering of 67.61 *epfu* and the total refined site-scattering equals 63.8 *epfu*. So we have a difference of 3.81 *epfu* in the total site-scattering values from EMPA and structure refinement. This difference of ~7% is possibly due to the cation and anion disorder in the structure of betalomonosovite. In the O sheet, there are two *Na*(1,2) sites, each with a refined scattering of 7.2 *epfu* which corresponds to 65% occupancy by Na of each site. Hence we assign 0.65 Na + 0.35 □ to each of the *Na*(1) and *Na*(2) sites, with the calculated site-scattering 7.15 *epfu*. By analogy with the *Na*(1,2) sites we assign 0.78 Na + 0.22 □ to each of the *Na*(3) and *Na*(4) sites (A^P sites of the TS block),

TABLE 6. FINAL ATOM COORDINATES AND DISPLACEMENT PARAMETERS (Å^2) FOR BETALOMONOSOVITE

Atom	*x*	*y*	*z*	U_{11}	U_{22}	U_{33}	U_{23}	U_{13}	U_{12}	U_{eq}
Ti(1)	0.2326(2)	0.31167(8)	0.00656(8)	0.0169(6)	0.0183(6)	0.0140(6)	0.0016(5)	0.0019(4)	0.0033(5)	0.0167(3)
Ti(2)	0.2475(2)	0.81204(8)	0.00714(8)	0.0166(6)	0.0184(6)	0.0132(6)	0.0020(5)	0.0026(4)	0.0043(5)	0.0163(3)
Ti(3)	0.15971(19)	0.47467(8)	0.22019(8)	0.0063(5)	0.0129(5)	0.0150(6)	0.0041(4)	0.0021(4)	0.0023(4)	0.0112(3)
Ti(4)	0.16166(19)	0.97461(8)	0.22028(8)	0.0066(5)	0.0124(5)	0.0149(6)	0.0039(4)	0.0016(4)	0.0026(4)	0.0111(3)
Si(1)	0.6395(3)	0.32954(12)	0.19940(12)	0.0093(8)	0.0111(9)	0.0111(9)	0.0019(7)	0.0018(6)	0.0012(6)	0.0105(4)
Si(2)	0.3454(3)	0.17043(12)	0.79992(12)	0.0097(8)	0.0107(8)	0.0113(9)	0.0024(7)	0.0007(6)	0.0022(6)	0.0106(4)
Si(3)	0.6445(3)	0.11209(13)	0.18206(13)	0.0139(9)	0.0116(9)	0.0137(9)	0.0045(7)	0.0034(7)	0.0030(7)	0.0127(4)
Si(4)	0.6628(3)	0.61226(13)	0.18296(13)	0.0125(9)	0.0118(9)	0.0136(9)	0.0042(7)	0.0014(7)	0.0024(7)	0.0124(4)
P(1)	0.2764(6)	0.12690(17)	0.44326(18)	0.0318(16)	0.0210(12)	0.0264(13)	–0.0026(10)	0.0041(10)	–0.0009(10)	0.0276(6)
P(2)	0.1791(6)	0.62577(17)	0.44387(17)	0.0231(15)	0.0227(13)	0.0223(12)	–0.0031(9)	0.0054(10)	0.0057(10)	0.0238(5)
P(3)	0.152(3)	0.1240(8)	0.4457(9)	0.033(4)						
P(4)	0.292(4)	0.6219(15)	0.4467(17)	0.050(7)						
Na(1)	0.2190(10)	0.0534(4)	0.0115(4)	0.039(3)	0.029(3)	0.044(3)	0.005(2)	–0.010(2)	0.008(2)	0.0389(13)
Na(2)	0.2264(10)	0.5545(4)	0.0147(4)	0.038(3)	0.026(3)	0.044(3)	0.003(2)	–0.014(2)	0.010(2)	0.0384(13)
Na(3)	0.1527(7)	0.2337(3)	0.2573(3)	0.0194(19)	0.032(2)	0.053(3)	0.023(2)	0.0049(18)	0.0025(16)	0.0325(10)
Na(4)	0.1828(8)	0.7355(3)	0.2595(3)	0.025(2)	0.030(2)	0.049(3)	0.019(2)	0.0069(18)	0.0017(17)	0.0326(10)
Na(5)	0.3300(8)	0.5068(3)	0.6267(3)	0.052(2)	0.038(2)	0.038(2)	–0.0076(16)	–0.0019(17)	0.0116(17)	0.0459(10)
Na(6)	0.2598(8)	0.0074(3)	0.6249(3)	0.067(3)	0.039(2)	0.032(2)	–0.0052(16)	0.0078(18)	–0.0066(19)	0.0481(10)
Na(7)	0.698(9)	0.231(3)	0.400(3)	0.06(3)	0.06(3)	0.03(2)	0.005(19)	–0.007(19)	–0.01(2)	0.052(11)
Na(8)	0.296(10)	0.269(5)	0.604(4)	0.04(3)	0.09(5)	0.04(3)	0.01(3)	–0.04(2)	–0.01(3)	0.058(17)
A(1)	0.2067(15)	0.8541(6)	0.3838(6)	0.031(4)	0.032(4)	0.036(4)	0.020(3)	0.002(3)	0.005(3)	0.0313(17)
A(2)	0.2160(18)	0.3570(6)	0.3869(6)	0.053(5)	0.029(4)	0.045(5)	0.026(4)	0.019(4)	0.015(4)	0.039(2)
O(1)	0.6193(11)	0.1000(4)	0.0671(4)	0.042(3)	0.019(3)	0.014(3)	0.006(2)	0.006(2)	0.006(2)	0.0244(12)
O(2)	0.6320(11)	0.5999(4)	0.0676(4)	0.043(3)	0.021(3)	0.014(3)	0.005(2)	0.004(2)	0.011(2)	0.0259(12)
O(3)	0.3879(11)	0.0800(4)	0.2143(4)	0.033(3)	0.035(3)	0.038(3)	0.004(3)	0.013(3)	–0.017(3)	0.0356(14)
O(4)	0.4443(11)	0.5563(4)	0.2161(4)	0.031(3)	0.038(3)	0.040(3)	0.011(3)	0.009(3)	–0.013(3)	0.0358(14)
O(5)	0.6872(10)	0.2273(3)	0.2314(4)	0.032(3)	0.013(2)	0.019(3)	0.005(2)	–0.003(2)	0.000(2)	0.0214(11)
O(6)	0.3567(10)	0.2732(3)	0.7674(3)	0.041(3)	0.010(2)	0.017(3)	0.004(2)	0.006(2)	0.004(2)	0.0223(11)
O(7)	0.3973(9)	0.3760(4)	0.2489(3)	0.016(2)	0.028(3)	0.015(2)	0.006(2)	0.0026(19)	0.013(2)	0.0196(11)
O(8)	0.5616(9)	0.1059(4)	0.7494(3)	0.021(3)	0.031(3)	0.01592)	0.003(2)	0.002(2)	0.017(2)	0.0224(11)
O(9)	0.8825(11)	0.0571(5)	0.2162(4)	0.035(3)	0.042(4)	0.039(3)	0.007(3)	0.004(3)	0.025(3)	0.0389(15)
O(10)	0.0611(10)	0.4199(4)	0.7841(4)	0.027(3)	0.032(3)	0.037(3)	0.006(3)	–0.000(2)	0.019(2)	0.0323(13)
O(11)	0.1112(9)	0.6051(4)	0.7570(3)	0.018(3)	0.030(3)	0.013(2)	0.001(2)	0.0021(19)	–0.012(2)	0.0213(11)
O(12)	0.0708(9)	0.1230(4)	0.7562(3)	0.020(3)	0.032(3)	0.011(2)	0.002(2)	0.0014(19)	–0.009(2)	0.0216(11)
O(13)	0.5826(9)	0.3055(3)	0.0828(3)	0.020(2)	0.017(2)	0.010(2)	–0.0009(18)	0.0044(18)	0.0013(19)	0.0160(10)
O(14)	0.5986(9)	0.8059(3)	0.0838(3)	0.016(2)	0.021(3)	0.011(2)	0.0013(19)	0.0035(18)	0.0008(19)	0.0163(10)
O(15)	0.1274(9)	0.4222(4)	0.0910(3)	0.020(2)	0.020(3)	0.012(2)	0.0022(19)	0.0024(19)	0.000(2)	0.0175(10)
O(16)	0.1437(9)	0.9218(4)	0.0919(3)	0.022(3)	0.023(3)	0.015(2)	0.004(2)	0.004(2)	0.003(2)	0.0197(10)

TABLE 6. (CONTINUED) FINAL ATOM COORDINATES AND DISPLACEMENT PARAMETERS (Å^2) FOR BETALOMONOSOVITE

Atom	*x*	*y*	*z*	U_{11}	U_{22}	U_{33}	U_{23}	U_{13}	U_{12}	U_{eq}
O(17)	0.0941(9)	0.7154(3)	0.0712(3)	0.019(2)	0.016(2)	0.015(2)	0.0037(19)	0.0017(19)	0.0021(19)	0.0167(10)
O(18)	0.0781(9)	0.2147(3)	0.0703(3)	0.019(2)	0.017(2)	0.014(2)	0.0027(19)	0.0009(19)	0.0002(19)	0.0169(10)
O(19)	0.1950(10)	0.0338(4)	0.3727(4)	0.029(3)	0.034(3)	0.024(3)	0.003(2)	0.006(2)	–0.000(2)	0.0292(12)
O(20)	0.2184(11)	0.5333(4)	0.3735(4)	0.034(3)	0.034(3)	0.023(3)	0.001(2)	0.005(2)	0.008(2)	0.0312(13)
O(21)	0.1620(16)	0.1299(6)	0.5360(6)	0.051(2)						
O(22)	0.5694(16)	0.1190(6)	0.4687(6)	0.05						
O(23)	0.2387(18)	0.2207(7)	0.4139(7)	0.049(2)						
O(24)	0.0994(8)	0.3822(7)	0.5305(6)	0.056(2)						
O(25)	0.3540(17)	0.6284(6)	0.5354(6)	0.052(2)						
O(26)	0.2096(18)	0.7199(6)	0.4159(7)	0.049(2)						
O(27)	0.145(7)	0.198(3)	0.383(3)	0.017(7)						
O(28)	–0.105(4)	0.123(3)	0.473(3)	0.028(9)						
O(29)	0.351(7)	0.129(3)	0.539(2)	0.038(10)						
O(30)	0.173(8)	0.617(3)	0.539(3)	0.032(9)						
O(31)	0.287(8)	0.702(2)	0.387(3)	0.026(9)						
O(32)	0.568(4)	0.624(4)	0.469(4)	0.05						

with the calculated site-scattering 8.6 *epfu* each. Now we are left with 2.53 Na + 0.36 Ca + 0.04 Mn + 0.01 Mg = 2.94 *apfu* to assign to six alkali-cation sites in the **I** block. Based on the refined site-scattering for the *Na*(5) and *Na*(6) sites, we assign 1.00 Na to each of these sites. After that we are left with 0.53 Na + 0.36 Ca + 0.04 Mn + 0.01 Mg = 0.94 *apfu* to assign to four alkali-cation sites: *Na*(7,8) and *A*(1,2). There are short distances involving several sites in the **I** block: *Na*(3)–*A*(2) = 2.25 and *Na*(4)–*A*(1) = 2.16 Å (Table 7). Hence the *Na*(3,4) and *A*(1,2) sites must be partly occupied and their site-occupancy sums, Na(3) + A(1) and Na(4) + A(2), must be ≤ 100%. As the *Na*(3,4) sites are each 78% occupied by Na, the *A*(1) and *A*(2) sites must have an occupancy ≤22%. The total refined site-scattering for both *A*(1) and *A*(2) sites is 8.8 *epfu*, which corresponds to 0.8 Na *apfu* with site occupancies of 40%. First, the latter site occupancy cannot occur (*cf.* requirement of ≤22% above), and second, we do not have enough Na for this assignment. Hence we assign 0.78 □ + 0.18 Ca + 0.02 Mn + 0.02 Na to each of the *A*(1,2) sites, and the total calculated site-scattering is 8.64 *epfu*. In accord with the refined site-scattering, we assign 0.86 □ + 0.14 Na to each of the *Na*(7,8) sites.

Finally, we consider the *P* sites in the **I** block. The short distances P(1)–P(3) = 0.67 and P(2)–P(4) = 0.60 Å tell us that these sites can be only partly occupied by P. In accord with the refined site-scattering, we assign 0.86 P + 0.14 □ to each of the *P*(1,2) sites and 0.86 □ + 0.14 P to each of the *P*(3,4) sites.

Description of the Structure

Betalomonosovite belongs to Group IV of the TS-block minerals (Sokolova 2006). Sokolova (2006) wrote the following general formula for the TS block within the planar cell based on t_1 and t_2 translations (Group IV), $A^P_2M^H_2M^O_4(Si_2O_7)_2X_{4+n}$, where M^O are cations of the O sheet, M^H are [6]-coordinated cations of the H sheet, and A^P are cations at the peripheral (*P*) sites, $X_{4+n} = X^O_4 + X^P_{M2} + X^P_{A2}$, where X^O_4 anions are common vertices of M^O octahedra and two M^H and two A^P polyhedra (they are the X^O_M and X^O_A anions), and anions X^P_M and X^P_A belong to the M^H and A^P polyhedra on the outside of the TS block (in the intermediate space between two TS blocks); n is the number of X^P anions: n = 2–4 in Group IV. There are two types of chains of edge-sharing octahedra within the O sheet: the Ti octahedra form a brookite-like $(Ti_2O_8)^{8-}$ chain, and the Na octahedra form a chain of the same topology (Fig. 5a). In the H sheet, Ti-dominant M^H octahedra link to Si_2O_7 groups and [8]-coordinated Na atoms occupy the A^P sites (Fig. 5b). In Group IV, linkage 3 occurs, and two Si_2O_7 groups link to two next-nearest-neighbor Ti

TABLE 7. SELECTED INTERATOMIC DISTANCES (Å) AND ANGLES (°) IN BETALOMONOSOVITE

Ti(1)–O(15)	1.885(5)	Ti(2)–O(16)	1.878(5)	Ti(3)–O(15)	1.841(5)	Ti(4)–O(16)	1.834(5)
Ti(1)–O(17)*a	1.954(5)	Ti(2)–O(18)*a	1.947(5)	Ti(3)–O(10)d	1.914(5)	Ti(4–O(9)e	1.902(6)
Ti(1)–O(2)c	2.006(5)	Ti(2)–O(1)c	1.998(5)	Ti(3)–O(4)	1.918(6)	Ti(4)–O(3)f	1.938(5)
Ti(1)–O(18)*	2.039(5)	Ti(2)–O(17)*	2.037(5)	Ti(3)–O(11)d	1.933(5)	Ti(4)–O(8)b	1.943(5)
Ti(1)–O(13)	2.075(5)	Ti(2)–O(14)	2.083(5)	Ti(3)–O(7)	1.975(5)	Ti(4)–O(12)d	1.964(5)
Ti(1)–O(14)c	2.142(5)	Ti(2)–O(13)c	2.140(5)	Ti(3)–O(20)	2.176(6)	Ti(4)–O(19)f	2.166(5)
<Ti(1)–O>	2.017	<Ti(2)–O>	2.014	<Ti(3)–O>	1.960	<Ti(4)–O>	1.958
Si(1)–O(11)b	1.601(5)	Si(2)–O(12)	1.610(5)	Si(3)–O(9)b	1.585(6)	Si(4)–O(4)	1.583(6)
Si(1)–O(7)	1.617(5)	Si(2)–O(8)	1.611(5)	Si(3)–O(3)	1.591(6)	Si(4)–O(10)b	1.599(5)
Si(1)–O(5)	1.632(5)	Si(2)–O(6)	1.633(5)	Si(3)–O(1)	1.628(5)	Si(4)–O(6)b	1.628(5)
Si(1)–O(13)	1.641(5)	Si(2)–O(14)b	1.636(5)	Si(3)–O(5)	1.630(5)	Si(4)–O(2)	1.633(5)
<Si(1)–O>	1.622	<Si(2)–O>	1.623	<Si(3)–O>	1.609	<Si(4)–O>	1.611
Si(1)–O(5)–Si(3)	134.0(3)	Si(2)–O(6)–Si(4)e	134.0(3)				
P(1)–^{a}O(23)	1.493(9)	P(2)–^{a}O(26)	1.494(9)	P(3)–^{b}O(28)	1.470(1)	P(4)–O(20)	1.47(2)
P(1)–O(19)	1.503(6)	P(2)–O(20)	1.498(6)	P(3)–O(19)	1.500(1)	P(4)–^{b}O(32)	1.470(1)
P(1)–^{a}O(21)***	1.529(9)	P(2)–^{a}O(25)***	1.530(9)	P(3)–^{b}O(27)	1.51(1)	P(4)–^{b}O(30)	1.56(5)
P(1)–^{a}O(22)**	1.576(9)	P(2)–^{a}O(24)**d	1.580(1)	P(3)–^{b}O(29)**	1.610(1)	P(4)–^{b}O(31)**	1.570(1)
<P(1)–O>	1.525	<P(2)–O>	1.526	<P(3)–O>	1.541.52	<P(4)–O>	1.52
Na(1)–O(1)	2.238(8)	Na(2)–O(2)	2.254(8)	Na(3)–^{a}O(23)	2.32(1)	Na(4)–^{a}O(26)	2.31(1)
Na(1)–O(16)a	2.393(7)	Na(2)–O(15)a	2.370(7)	Na(3)–O(7)	2.430(7)	Na(4)–O(12)d	2.464(7)
Na(1)–O(18)*	2.405(7)	Na(2)–O(17)*	2.379(7)	Na(3)–O(5)i	2.468(6)	Na(4)–O(10)d	2.470(7)
Na(1)–O(1)g	2.424(7)	Na(2)–O(2)c	2.410(7)	Na(3)–O(3)	2.507(8)	Na(4)–O(6)b	2.528(7)
Na(1)–O(16)h	2.468(8)	Na(2)–O(15)	2.466(7)	Na(3)–O(18)*	2.650(7)	Na(4)–O(8)b	2.659(7)
<Na(1)–O>	2.386	<Na(2)–O>	2.376	Na(3)–O(11)d	2.725(7)	Na(4)–O(17)*	2.669(7)
				<Na(3)–O>	2.516	<Na(4)–O>	2.517
Na(5)–^{a}O(24)**	2.248(9)	Na(6)–^{a}O(22)**j	2.250(9)	A(1)–^{b}O(28)d	2.16(3)	A(2)–^{b}O(32)b	2.24(4)
Na(5)–^{b}O(32)	2.16(5)	Na(6)–^{b}O(28)k	2.15(4)	A(1)–^{b}O(31)**	2.22(3)	A(2)–^{b}O(27)	2.27(4)
Na(5)–^{a}O(25)***	2.41(1)	Na(6)–^{a}O(21)***	2.41(1)	A(1)–O(12)	2.462(9)	A(2)–O(7)	2.385(9)
Na(5)–^{b}O(30)	2.33(4)	Na(6)–^{b}O(29)	2.42(4)	A(1)–^{b}O(29)**b	2.49(3)	A(2)–^{b}O(30)d	2.43(4)
Na(5)–O(20)b	2.443(1)	Na(6)–O(8)	2.447(6)	A(1)–O(8)b	2.568(9)	A(2)–O(20)f	2.55(1)
Na(5)–O(7)b	2.445(1)	Na(6)–O(19)k	2.498(7)	A(1)–O(19)f	2.588(9)	< A(2)–O>	2.38
Na(5)–O(11)	2.486(6)	Na(6)–O(12)	2.519(6)	< A(1)–O>	2.42		
Na(5)–O(4)b	2.791(7)	Na(6)–O(9)j	2.840(8)				
<Na(5)–O>	2.471[a]	<Na(6)–O>	2.494[a]	short distances			
	2.443[b]		2.479[b]	P(1)–P(3)	0.67(1)	P(2)–P(4)	0.60(2)
				Na(3)–A(2)	2.25(1)	Na(4)–A(1)	2.16(1)
Na(7)–^{b}O(30)b	2.20(6)	Na(8)–^{b}O(29)**	2.04(8)	^{a}O(21)–^{b}O(28)	1.60(3)	^{a}O(21)–^{b}O(29)**	1.01(4)
Na(7)–^{b}O(28)l	2.26(6)	Na(8)–^{b}O(32)b	2.19(9)	^{a}O(22)–^{b}O(28)	1.73(2)	^{a}O(22)–^{b}O(29)**	1.61(5)
Na(7)–O(5)	2.43(4)	Na(8)–^{b}O(31)**b	2.24(7)	^{a}O(23)–^{b}O(27)	0.66(4)	^{a}O(24)–^{b}O(30)d	1.68(4)
Na(7)–^{b}O(27)l	2.46(6)	Na(8)–O(6)l	2.34(6)	^{a}O(24)–^{b}O(32)b	1.78(2)	^{a}O(25)–^{b}O(30)	0.99(4)
<Na(7)–O>	2.34	<Na(8)–O>	2.20	^{a}O(25)–^{b}O(32)	1.57(4)	^{a}O(26)–^{b}O(31)**	0.63(4)

Symmetry operators: a: $-x$, $-y+1$, $-z$; b: $-x+1$, $-y+1$, $-z+1$; c: $-x+1$, $-y+1$, $-z$; d: $-x$, $-y+1$, $-z+1$; e: $x-1$, $y+1$, z; f : x, $y+1$, z; g: $-x+1$, $-y$, $-z$; h: x, $y-1$, z; i: $x-1$, y, z; j: $-x+1$, $-y$, $-z+1$; k: $-x$, $-y$, $-z+1$; l: $x+1$, y, z.
*(O,F,OH); **OH; ***(O,OH); [a, b] = anion site is occupied at 86 and 14%, respectively [*e.g.*, [a]O(24) = 86% occupied].
For the Na(5,6) octahedra, two mean bond-lengths are given (depending on anion sites partly occupied by O atoms at 86 and 14%); *e.g.*, Na(5): 2.471[a] and 2.443[b] Å correspond to 6 fully occupied anion sites plus O(24,25) occupied by O atoms at 86% and 6 fully occupied anion sites plus O(30,32) occupied by O atoms at 14%.

octahedra in a brookite-like chain along **a** (= $\mathbf{t}_1$) (Figs. 5a, 5c).

Cation sites

The structure of betalomonosovite consists of two types of block (TS and **I**) alternating along [001]. We describe the cation sites of the TS block (O and H sheets, peripheral sites) and the cation sites of the **I** block.

The O sheet. There are four cations sites octahedrally coordinated by O atoms and (O,F,OH) anions at the O(17,18) sites (Fig. 5a). The two Ti-dominant sites, *Ti*(1,2), are occupied by ($Ti_{1.24}Nb_{0.24}Mg_{0.29}Mn_{0.20}Zr_{0.02}Ta_{0.01}$) and coordinated by four O atoms and two (O,F,OH) anions,

with <Ti(1)–O> = 2.017 and <Ti(2)–O> = 2.014 Å. The mean observed bond-lengths are in good agreement with calculated bond-lengths: 2.027 Å (Table 8). The *Na*(1,2) sites are each occupied by ($Na_{0.65}\square_{0.35}$) and coordinated by four O atoms and an (O,F,OH) anion: Na(1,2)–O distances vary from 2.238 to 2.468 Å, with <Na(1)–O> = 2.386 and <Na(2)–O> = 2.378 Å (Table 7). The Na(1,2) atoms each have the sixth anion at a significantly longer distance: Na(1)–O(14) = 2.893 and Na(2)–O(13) = 2.925 Å [*cf.* Na(2)–O(5) = 2.696 Å in lomonosovite]. Betalomonosovite is the only Group-IV TS-block mineral that has [5]-coordinated Na in the O sheet. For the O sheet, the total of the four cations is $(Na_{0.65}\square_{0.35})_2(Ti_{1.24}Nb_{0.24}Mg_{0.29}Mn_{0.20}Zr_{0.02}Ta_{0.01})$, with simplified and ideal compositions $(Na,\square)_2(Ti,M^{2+})$ where M^{2+} = Mg, Mn and Na_2Ti_2 *apfu*, respectively.

The H sheet. The *Ti*(3,4) (=M^H) sites are occupied primarily by Ti (Table 8) and are octahedrally coordinated by O atoms. The Ti–O distances vary from 1.834 to 2.176 Å with <Ti(1)–O> = 1.960 and <Ti(2)–O> = 1.958 Å [*cf.* calculated bond-lengths of 1.986 Å (Table 8)]. There are four tetrahedrally coordinated sites occupied by Si, with a grand <<Si–O>> distance of 1.617 Å. For the two H sheets, the total of the two octahedrally coordinated cations is $(Ti_{1.53}Nb_{0.24}Fe^{3+}_{0.23})_{\Sigma 2}$, with simplified and ideal compositions Ti_2 *apfu*. Si_2O_7 groups will be considered as complex oxyanions.

The peripheral (P) sites. The [6]-coordinated *Na*(3,4) (=A^P) sites are partly occupied by Na: [2 × ($Na_{0.78}\square_{0.02}$)] *apfu*, with <Na(3)–O> = 2.516 Å and <Na(4)–O> = 2.517 Å (Tables 5 and 6). The total of two cations is $(Na_{0.78}\square_{0.22})_{\Sigma 2}$, with simplified and ideal compositions $(Na,\square)_2$ and Na_2 *apfu*, respectively.

The ***I*** *block.* There are two *P* sites, each of which splits into two sites: the first *P* site splits into the *P*(1) and *P*(3) sites separated by 0.67 Å, and the second site splits into the *P*(2) and *P*(4) sites separated by 0.60 Å. The *P*(1) and *P*(2) sites are occupied by P at 86% and are tetrahedrally coordinated by two O atoms, one OH group, and one anion of average composition $[O_{0.5}(OH)_{0.5}]$ [a detailed explanation of the anion composition and stoichiometry of the P tetrahedra follows in the sections *Anion considerations* and *Short-Range Order (SRO)*], with <P(1)–O> = 1.525 Å, P(1)–O(22)OH = 1.576 Å, P(1)–O(21)$[O_{0.5}(OH)_{0.5}]$ = 1.529 Å, and <P(2)–O> = 1.526 Å, P(2)–O(24)OH = 1.576 Å, P(2)–O(25)$[O_{0.5}(OH)_{0.5}]$ = 1.530 Å. We write the composition of the P(1,2) tetrahedra as follows: 2 × 0.86$[PO_2O_{0.5}(OH)_{0.5}(OH)]$ = 2 × 0.86$[PO_{2.5}(OH)_{1.5}]$ = 0.86{$[PO_3(OH)][PO_2(OH)_2]$} *pfu*. The *P*(3) and *P*(4) sites are occupied by P at 14% and tetrahedrally coordinated by O atoms which occur at the O sites occupied at 14%. Table 7 reports following bond-lengths for the P(3,4) tetrahedra: <P(3)–O> = 1.52, P(3)–O(29)OH = 1.610 Å and <P(4)–O> = 1.52, P(4)–O(31)OH = 1.570 Å. We are unable to identify P–$[O_{0.5}(OH)_{0.5}]$ distances for the P(3,4) tetrahedra, and it is difficult to make suggestions on the stoichiometry of the P(3,4) tetrahedra based on P–O distances (the electron count at the corresponding O sites is ~0.28 *el*). We consider the P(3,4) tetrahedra of the same stoichiometry as the P(1,2) tetrahedra: the P(3,4) tetrahedra give 0.14{$[PO_3(OH)][PO_2(OH)_2]$} *pfu*. In the **I** block, there are six alkali cation sites. The [6]-coordinated *Na*(5,6) sites are occupied solely by Na. Each of the Na(5,6) atoms can be coordinated by (1) O atoms which occur at sites with 100 and 86% occupancies, and (2) O atoms which occur at sites with 100 and 14% occupancies, and have corresponding <Na(5)–O> = (1) 2.471 and (2) 2.443 Å, and <Na(6)–O> = (1) 2.494 and (2) 2.479 Å (Table 7). There are four sites occupied primarily by vacancies (□). The [4]-coordinated *Na*(7,8) sites are partly occupied by Na, giving $(\square_{0.86}Na_{0.14})_2$ *pfu*, with <Na(7)–O> = 2.34 and <Na(8)–O> = 2.20 Å. The [6]-coordinated *A*(1) and [5]-coordinated *A*(2) sites are partly occupied by Ca with minor Mn and Na, giving $(\square_{0.78}Ca_{0.18}Mn_{0.02}Na_{0.02})_2$ *pfu*, with <A(1)–O> = 2.42 and <A(2)–O> = 2.38 Å. Cations at the four *Na* and two *A* sites of the **I** block sum to $Na_2[Na(5,6)]$ + $(\square_{0.86}Na_{0.14})_2[Na(7,8)]$ + $(\square_{0.78}Ca_{0.18}Mn_{0.02}Na_{0.02})_2$ [*A*(1,2)] = $(\square_{3.28}Na_{2.32}Ca_{0.36}Mn_{0.04})$ *pfu*. Ideally, the four *Na* and two *A* sites of the **I** block give Na_2 [*Na*(5,6)] + $\square_2[Na(7,8)]$ + $\square_2$ [*A*(1,2)] = $Na_2\square_4$ *pfu*. $PO_3(OH)$ and $PO_2(OH)_2$ groups will be considered as complex oxyanions (see *Anion considerations* below).

We write the ideal cation part of the structure as the sum of $Na_2\square_4$(**I** block) + Na_2Ti_2(O sheet) + Ti_2(H sheets) + $Na_2(A^P{}_2)$ = $Na_6\square_4Ti_4$ *apfu*, with a charge of 22+.

Anion considerations

Table 9 lists the bond-valence values for all anions.

The anion sites with full occupancy. Fourteen anions, O(1–14), with bond-valence sums 1.86–2.12 *vu*, belong to Si_2O_7 groups and are O atoms, giving $(Si_2O_7)_2$ *pfu*. Two anions, O(15,16) [= $X^O{}_M$], each receive bond valence from one Ti atom in the H sheet and one Ti atom and two Na(1,2) atoms in the O sheet; their bond-valence sums are 1.99 and 2.04 *vu*, respectively, and they are O atoms, giving O_2 *apfu*. Table 9 gives incident bond-valences of 1.37 and 1.47 *vu* for the O(17,18) [= $X^O{}_A$] anions. The $X^O{}_A$ atom receives bond valence from two Ti(1,2) atoms in the O sheet, one of the Na(1,2) atoms in the O sheet, and one of the Na(3,4) atoms in the H sheet (Figs. 5a, 5c). Note that the *Na*(1,2) and *Na*(3,4) sites are 65% and 78% occupied by Na (Tables 6, 7). Hence the bond-valence sums at the O(17,18) anions vary depending on whether the *Na*(1,2) and *Na*(3,4) sites are locally occupied by Na or are vacant.

TABLE 8. REFINED SITE-SCATTERING (*epfu*) AND ASSIGNED SITE-POPULATIONS (*apfu*) FOR BETALOMONOSOVITE*

Site**			Refined site-scattering	Site population	Calculated site-scattering	<X–φ>$_{calc.}$ (Å)	<X–φ>$_{obs.}$ (Å)
1	2	3					
Ti(1)	M^O	*Ti*(2)	23.8(1)	1.24 Ti + 0.29 Mg + 0.24 Nb +	47.13	2.027	2.017
Ti(2)	M^O		23.8(1)	0.20 Mn^{2+} + 0.02 Zr + 0.01 Ta		2.027	2.014
Ti(3)	M^H	*Ti*(1)	23.8(1)	11.53 Ti + 0.24 Nb +	49.48	1.986	1.960
Ti(4)	M^H		23.8(1)	0.23 Fe^{3+}		1.986	1.958
[4]*P*(1)		*P*	12.9(2)	0.86 P + 0.14 □	12.9	1.523	1.525
[4]*P*(2)			12.9(2)	0.86 P + 0.14 □	12.9	1.523	1.526
[4]*P*(3)			2.1(2)	0.86 □ + 0.14 P	2.1		1.52
[4]*P*(4)			2.1(2)	0.86 □ + 0.14 P	2.1		1.52
[5]*Na*(1)	M^O	*Na*(2)	7.2(1)	0.65 Na + 0.35 □	7.15	2.373	2.386
[5]*Na*(2)	M^O		7.2(1)	0.65 Na + 0.35 □	7.15	2.373	2.378
Na(3)	A^P	[8]*Na*(1)	8.6(1)	0.78 Na + 0.22 □	8.6	2.384	2.516
Na(4)	A^P		8.6(1)	0.78 Na + 0.22 □	8.6	2.384	2.517
ΣNa (TS block)			31.6	2.86 Na + 1.14 □	31.5		
Na(5)		*Na*(3)	11.0(3)	1.00 Na	11.0	2.379	2.471[a] 2.443[b]
Na(6)			11.0(3)	1.00 Na	11.0	2.379	2.494[a] 2.479[b]
[4]*Na*(7)		[4]*Na*(4)	1.0(2)	0.86 □ + 0.14 Na	1.54		2.34
[4]*Na*(8)			0.8(2)	0.86 □ + 0.14 Na	1.54		2.20
A(1)		[5]*Na*(5)	4.4(2)	0.78 □ + 0.18 Ca + 0.02 Mn^{2+} + 0.02 Na	4.32		2.42
[5]*A*(2)			4.4(2)	0.78 □ + 0.18 Ca + 0.02 Mn^{2+} + 0.02 Na	4.32		2.38
ΣNa (I block)			32.6	2.32 Na + 0.36 Ca + 0.04 Mn^{2+} + 3.28 □	33.72		

* X = cation; φ = unspecified anion, φ = O, OH, F; <X–φ> calculated for cation sites with >50% occupancy using ionic radii of Shannon (1976); coordination number is shown in brackets for non-octahedral sites;
** 1: in accord with cation sites of Rastsvetaeva (1986) used in this work, each site gives 1 *apfu*;
2: in accord with terminology of Sokolova (2006);
3: in accord with cation sites in lomonosovite of Cámara *et al.* (2008), after Belov *et al.* (1977), each site is fully occupied and gives 2 *apfu*;
[a] mean bond-lengths involving 100%- and 86%-occupied anion sites;
[b] mean bond-lengths involving 100%- and 14%-occupied anion sites.

Moreover, the *Ti*(1+2) sites have the composition ($Ti_{1.24}Nb_{0.24}Mg_{0.29}Mn_{0.20}Zr_{0.02}Ta_{0.01}$), which has a significant content of divalent cations: $Mg_{0.29}Mn_{0.20}$, *i.e.*, M^{2+} equals 0.49 *apfu* (*cf.* 0.38 *apfu* in lomonosovite, Cámara *et al.* 2008). Therefore the bond-valence contribution from the two Ti(1,2) atoms to the O(17,18) atoms is lower than that from the Ti(1+3) and Ti(2+4) atoms to the O(15,16) atoms: 1.22 and 1.14 *vu versus* 1.73 and 1.78 *vu*. Substitution of M^{2+} for Ti requires substitution of F for O: $Ti^{4+} + O^{2-} \leftrightarrow M^{2+} + F^-$. Hence F enters the O(17,18) sites, and its amount, $F_{0.65}$, at the O(17+18) sites correlates with the amount of M^{2+} at the *Ti*(1+2) sites: 0.49 *apfu*. The anions 0.65 F^- + 1.35 O^{2-} give an aggregate charge of 3.35^- for the two O(17,18) sites, which is equivalent to 1.68^- for each site. Bond-valence calculations give (1.37 + 1.47) / 2 = 1.42 *vu* for each site (Table 9). To achieve a better agreement between the calculated bond-valence sums (1.42 *vu*) and the aggregate charges, we assign 0.53 $(OH)^-$ to these two sites: the composition $[O_{0.82}F_{0.65}(OH)_{0.53}]^{2.82-}$ is in good agreement with the aggregate bond-valence sum at the two O(17,18) sites: 1.37 + 1.47 = 2.84 *vu*. We write the composition of the O(17+18) sites as $[O_{0.82}F_{0.65}(OH)_{0.53}]$, ideally (OF) *pfu*. The occurrence of OH groups in the O sheet of the TS block is supported by FTIR spectroscopy (see above). Table 9 gives 1.99 and 2.04 *vu* for the O(19,20) [= X^P_M]

TABLE 9. BOND-VALENCE* VALUES FOR BETALOMONOSOVITE

Atom Site occ. (%)	Si(1) 100	Si(2) 100	Si(3) 100	Si(4) 100	P(1) 86	P(2) 86	P(3) 14	P(4) 14	Ti(1) 100	Ti(2) 100	Ti(3) 100	Ti(4) 100	Na(1) 65	Na(2) 65	Na(3) 78	Na(4) 78	Na(5) 100	Na(6) 100	Na(7) 14	Na(8) 14	A(1) 22	A(2) 22	Σ
O(1)			0.98							0.60			0.13										1.88
													0.18										
O(2)				0.97					0.59					0.13									1.86
														0.18									
[3]O(3)			1.09									0.71			0.13								1.93
[3]O(4)				1.11							0.76						0.11						1.98
O(5)	0.97		0.98												0.14				0.03				2.13
O(6)		0.97		0.98												0.13				0.03			2.12
O(7)	1.01										0.64				0.16		0.19					0.07	2.07
O(8)		1.03										0.70				0.08		0.19			0.04		2.04
[3]O(9)			1.10									0.78						0.10					1.96
[3]O(10)				1.06							0.77					0.14							1.97
O(11)	1.06										0.73				0.09		0.18						2.06
O(12)		1.03										0.66				0.14		0.17			0.06		2.06
[3]O(13)	0.95								0.49	0.43													1.87
[3]O(14)		0.96							0.43	0.49													1.88
O(15)									0.81		0.92			0.14									1.99
														0.12									
O(16)										0.82		0.96	0.14										2.04
													0.12										
O(17)									0.68	0.45				0.14		0.10							1.37
O(18)									0.54	0.69			0.13		0.11								1.47
O(19)					1.19		0.19					0.40						0.17			0.04		1.99
O(20)						1.20		0.21			0.39						0.19					0.05	2.04
O(21)					1.10													0.17					
O(22)					0.97													0.23					
O(23)					1.22										0.19								
O(24)						0.95											0.23						
O(25)						1.10											0.17						
O(26)						1.28										0.19							
O(27)							0.19												0.03			0.05	
O(28)							0.21											0.05	0.04		0.07		
O(29)							0.14											0.03		0.06	0.03		

TABLE 9. (CONTINUED) BOND-VALENCE* VALUES FOR BETALOMONOSOVITE

Atom	Si(1)	Si(2)	Si(3)	Si(4)	P(1)	P(2)	P(3)	P(4)	Ti(1)	Ti(2)	Ti(3)	Ti(4)	Na(1)	Na(2)	Na(3)	Na(4)	Na(5)	Na(6)	Na(7)	Na(8)	A(1)	A(2)	Σ
Site occ. (%)	100	100	100	100	86	86	14	14	100	100	100	100	65	65	78	78	100	100	14	14	22	22	
O(30)								0.17									0.03		0.04			0.04	
O(31)								0.16												0.04	0.06		
O(32)								0.21									0.05			0.04		0.06	
Total	3.99	3.99	4.15	4.12	4.48	4.53	0.73	0.75	3.54	3.48	4.21	4.21	0.70	0.71	0.82	0.78	1.15	1.11	0.14	0.17	0.30	0.27	
Aggregate charge	4.00	4.00	4.00	4.00	4.30	4.30	0.70	0.70	3.63	3.63	4.00	4.00	0.65	0.65	0.78	0.78	1.00	1.00	0.14	0.14	0.42	0.42	

* bond-valence parameters (*vu*) are from Brown (1981); O(17) + O(18) give $[O_{0.82}F_{0.65}(OH)_{0.53}]$ *pfu*; coordination numbers are shown for non-[4]-coordinated O atoms with 100%-occupancy: O(1–20); bond-valence sums for O atoms at O(21–26) and O(27–32) sites, which are occupied at 86 and 14%, are not given here due to the uncertainty of coordination; bond-valence contributions from Na(5,6) atoms are at 86% to O(21,22,24,25) and at 14% to O(28,29,30,32).

anions which are common anions for the Ti(3,4) octahedra and P tetrahedra. Hence the O(19,20) anions are O atoms which belong to the P tetrahedra. Hence the anion sites (full occupancy), which do not belong to the P tetrahedra, sum to $(Si_2O_7)_2$[O(1–14)] + O_2 [O(15,16)] + $[O_{0.82}F_{0.65}(OH)_{0.53}]$[O(17,18)] = $(Si_2O_7)_2O_2[O_{0.82}F_{0.65}(OH)_{0.53}]$, ideally $(Si_2O_7)_2O_2$(OF) *pfu*.

The anion sites with partial occupancy. The *P*(1) and *P*(2) sites (occupied by P at 86%) are tetrahedrally coordinated by O(19) (full occupancy), O(21–23) (86% occupancy) and O(20) (full occupancy), O(24–26) (86% occupancy), respectively (Table 6). In each of the P(1) and P(2) tetrahedra, there is one long bond: P(1)–O(22) = P(2)–O(24) = 1.58 Å (Table 7) and we assign an OH group to the O(22) and O(24) sites (Table 6). The *P*(3) and *P*(4) sites are occupied by P at 14% and are tetrahedrally coordinated by O(19) (full occupancy), O(27–29) (14% occupancy) and O(20) (full occupancy), O(30–32) (14% occupancy), respectively (Table 7). By analogy with P(1,2) tetrahedra, we assign an OH group to the O(29) and O(31) sites (Table 6). Consideration of the short-range order of atoms in the **I** block will be outlined later in the paper; here, we write the formulae of P(1–2) tetrahedra on the assumptions that (1) O(19) and O(20) belong to the P(1,2) and P(3,4) tetrahedra at 86 and 14%, respectively; (2) O(21) [P(1)] and O(25) [P(2)] are aggregate anions of composition $[O_{0.5}(OH)_{0.5}]$; and (3) the chemical compositions of the P(1,2) and P(3,4) tetrahedra are the same except for the site occupancies: 86 and 14%, respectively. We write the sum of the P(1,2) and P(3,4) tetrahedra as follows: 2 × 0.86$[PO_2O_{0.5}(OH)_{0.5}(OH)]$ + 2 × 0.14 $[PO_2O_{0.5}(OH)_{0.5}(OH)]$ = $[PO_3(OH)][PO_2(OH)_2]$. We write the anion part of the structure as the sum of $(Si_2O_7)_2$ + $[PO_3(OH)][PO_2(OH)_2]$ + O_2[O(15,16) = $(X^O_M)_2$] + (OF) [O(17,18) = $(X^O_A)_2$] = $(Si_2O_7)_2$ $[PO_3(OH)][PO_2(OH)_2]O_2$(OF) (charge = 22–). The total number of anions is 26 (O+F) *apfu*.

We write the ideal formula of betalomonosovite as the sum of the cation and anion parts, $Na_6\square_4$ $Ti_4(Si_2O_7)_2[PO_3(OH)][PO_2(OH)_2]O_2(OF)$, $Z = 2$.

Short-Range Order (SRO)

There are 22 cation sites in the crystal structure of betalomonosovite and 12 of them are partly occupied (Table 6). Two *Na*(1,2) sites, 65% occupied by Na, occur in the O sheet of the TS block (Fig. 5a). Two *Na*(3,4) [= A^P_2] sites, 78% occupied by Na, occur in the H sheet of the TS block (Fig. 5b). Eight partly occupied sites occur in the **I** block: *P*(1–4), *Na*(7,8), and *A*(1,2) (Table 8). Hence most of the alkali-cation sites and all of the *P* sites are partly occupied by Na (plus minor Ca) and P, respectively. In the **I** block, there are short distances P(1)–P(3), P(2)–P(4),

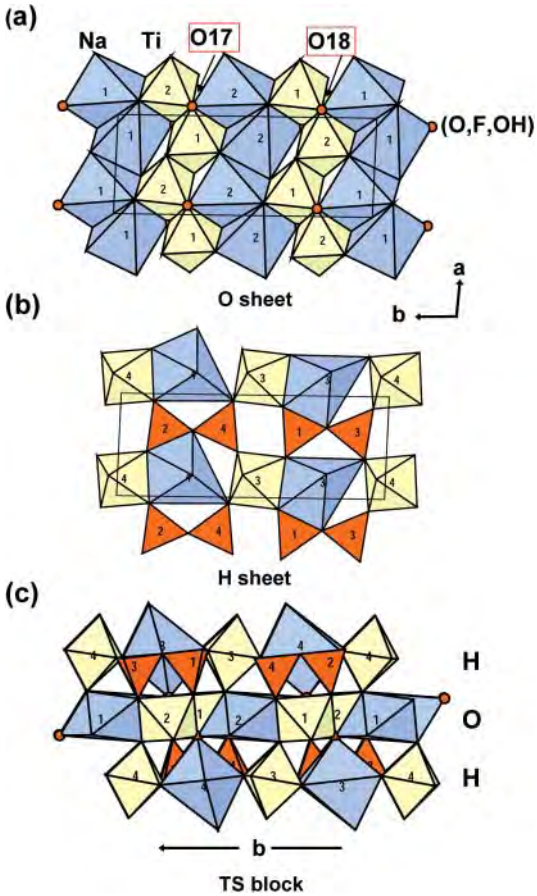

FIG. 5. The TS block in betalomonosovite; general view of (a) the sheet of octahedra (O sheet) and (b) the heteropolyhedral sheet (H sheet); (c) linkage of O and H sheets viewed down **a**. Ti octahedra are yellow, SiO_4 tetrahedra are orange, Na polyhedra are blue, and (O, F, OH) anions at the O(17) and O(18) sites are shown as orange spheres. Numbers 1–4 on yellow, 1–4 on blue, and 1–4 on orange correspond to Ti(1–4), Na(1–4) polyhedra, and Si(1–4) tetrahedra; thin black lines show the unit cell.

Na(3)–A(2), and Na(4)–A(1) (Table 7) which tell us that these cations occur at mutually exclusive sites at short range and that SRO of cations must occur. For better understanding of the topology of the **I** block, we propose two SRO models for its cations.

SRO-1. Consider first the cation sites associated with the *P*(1,2) sites in the **I** block. The P(1,2) tetrahedra (86% occupancy) share common vertices with Ti(3,4) octahedra (100%), [6]-coordinated Na(5,6) polyhedra (100%), and [6]-coordinated Na(3,4) [= A^P] polyhedra (78%) (Fig. 6a). Note that this SRO arrangement occurs when all constituent cation sites (next-nearest-neighbors) are locally fully occupied. In this SRO arrangement, the Na(5) and Na(6) atoms are each bonded to four O atoms (100% occupancy) and two O atoms (86% occupancy), and the mean bond-lengths are <Na(5)–O> = 2.471 Å and <Na(6)–O> = 2.494 Å (Table 7). Table 10 gives bond-valence values for the local arrangement of the P(1) and P(2) tetrahedra. Note that there are suitable distances for hydrogen bonds involving O atoms and OH groups of the P(1,2) tetrahedra: O(22)OH–O(26) = O(24)OH–O(23) = 2.68(1) Å. The bond-valence contribution of the H atoms to the acceptor O(23,26) atoms is 0.25 *vu* (Brown & Altermatt 1985) and possible H(1,2) atoms are included in Table 10 to account for hydrogen bonding. Table 10 shows that the P(1,2) atoms are each coordinated by two O atoms: O(19,20) (1.95 and 1.98 *vu*) and O(23,26) (2.03 and 2.10 *vu*), respectively; and one OH group: O(22,24) (2.16 and 2.13 *vu*, including 0.75 *vu* from an H atom). The bond-valence sums at O(21) and O(25) are 1.48 *vu*, which indicate that these anions are occupied by $O_{0.5}(OH)_{0.5}$ due to short-range order of cations in the second coordination sphere (next-next-nearest neighbors). This suggestion is supported by a second set of suitable distances for hydrogen bonds between O atoms and OH groups of the P(1,2) tetrahedra: O(21)OH–O(26) = 2.94(1) and O(25)OH–O(23) = 2.95(1) Å. We write the composition of the P(1,2) tetrahedra as follows: 2 × 0.86 $[PO_2O_{0.5}(OH)_{0.5}(OH)]$ = 2 × 0.86 $[PO_{2.5}(OH)_{1.5}]$ *pfu*. The two $PO_{2.5}(OH)_{1.5}$ groups tell us that there is very strong probability of occurrence of two types of P tetrahedra in the structure of betalomonosovite: $PO_3(OH)$ and $PO_2(OH)_2$. Hence we can write the composition of the P(1,2) tetrahedra 2 × 0.86 $[PO_2O_{0.5}(OH)_{0.5}(OH)]$ = 2 × 0.86 $\{[PO_3(OH)][PO_2(OH)_2]\}$. Figure 6b shows how P(1) and P(2) tetrahedra connect via hydrogen bonds to form a chain along **a**.

SRO-2. Consider the cation sites associated with the *P*(3,4) sites in the **I** block. By analogy with the *P*(1,2) sites, the *P*(3,4) sites are each 14% occupied by P and the P(3,4) atoms are each coordinated by two O atoms (100% and 14% occupancy), an OH group [O(29,31), 14% occupancy], and an aggregate anion $O_{0.5}(OH)_{0.5}$ (14% occupancy) (Table 7). The P(3,4) tetrahedra share common vertices with Ti(3,4) octahedra (100%), [6]-coordinated Na(5,6) polyhedra (100%), [6,5]-coordinated A(1,2) polyhedra (22%), and [4]-coordinated Na(7,8) polyhedra (Fig. 6c). In this SRO arrangement, the Na(5) and Na(6) atoms are each bonded to four O atoms (100% occupancy) and two O atoms (14% occupancy), Na(5)–O(30,32) and Na(6)–O(28,29), respectively, and the mean bond lengths are <Na(5)–O> = 2.443 and Na(6)–O> = 2.479 Å (Table 7). The A(1) and A(2) atoms are each bonded to three and two O atoms (100% occupancy), respectively, and three O atoms (14% occupancy), with mean bond lengths of <A(1)–O> = 2.42 and

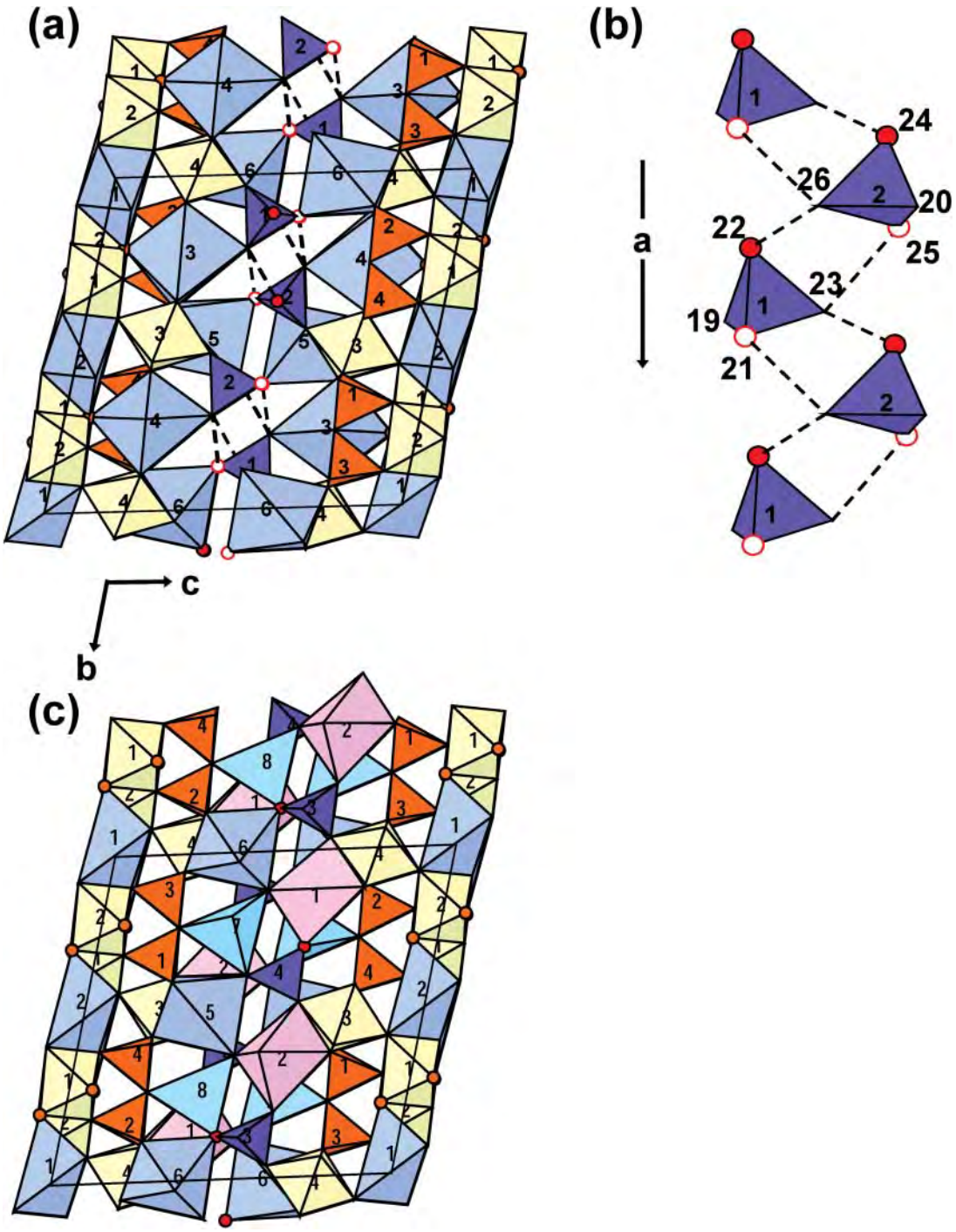

FIG. 6. Models of short-range order (SRO) for the cations in the **I** block of betalomonosovite: (a) SRO-1: cation sites with 78%, 86%, and 100% occupancy; (b) the disposition of the P tetrahedra connected by hydrogen bonds along **a**; (c) SRO-2: cation sites with 14%, 22%, and 100% occupancy. Legend as in Figure 3, P and A polyhedra are purple and pink; OH groups are shown as red spheres; in (a) and (b), $[O_{0.5}(OH)_{0.5}]$ anions at the O(21) and O(25) sites are shown as white spheres with red rims; hydrogen bonds are shown as black dashed lines; $PO_3(OH)$ and $PO_2(OH)_2$ tetrahedra occur where the O(21,25) sites are occupied by O and OH groups, respectively.

TABLE 10. BOND-VALENCE* VALUES FOR THE LOCAL (SHORT-RANGE ORDER) ARRANGEMENT OF THE P(1) AND P(2) TETRAHEDRA IN BETALOMONOSOVITE

Atom Site occ. (%)	P(1) 100	P(2) 100	Ti(3) 100	Ti(4) 100	Na(3) 100	Na(4) 100	Na(5) 100	Na(6) 100	H(1) 100	H(2) 100	Σ
O(19)	1.38			0.40				0.17			1.95
O(20)		1.40	0.39				0.19				1.98
O(21)[$O_{0.5}(OH)_{0.5}$]	1.28							0.20			1.48
O(22)(OH)	1.13							0.27	0.75		2.16
O(23)	1.42				0.24					0.25	2.03
O(24)(OH)		1.11					0.27			0.75	2.13
O(25)[$O_{0.5}(OH)_{0.5}$]		1.28					0.20				1.48
O(26)		1.49				0.24			0.25		2.10
Total	5.21	5.28							1.00	1.00	

* bond-valence parameters (vu) are from Brown (1981) and Brown & Altermatt (1985).

<A(2)–O> = 2.38 Å (Table 7). As site occupancies for the *P*(3,4) sites and coordinating anion sites are low, we do not consider possible hydrogen bonding involving P tetrahedra for the SRO-2 arrangement of cations.

Structure topology

The crystal structure of betalomonosovite is an alternation of TS and **I** blocks (Fig. 7a) and is topologically similar to that of lomonosovite (Fig. 7b). In the **I** block of the crystal structure of betalomonosovite, [4]- to [6]-coordinated alkali-cation polyhedra and $PO_3(OH)$ and $PO_2(OH)_2$ tetrahedra share vertices and edges to form a framework. Nearly all cation polyhedra of the **I** block are partly occupied [except for Na(5,6) octahedra] (Table 8). In Figure 7a, atoms at sites with less than 50% occupancy are shown as spheres. In lomonosovite, all cation polyhedra are fully occupied and the **I** block comprises [4]- to [6]-coordinated Na polyhedra and PO_4 tetrahedra. In betalomonosovite and lomonosovite, the composition of the **I** block is $Na\square_2[PO_3(OH)][PO_2(OH)_2$ and $Na_6(PO_4)_2$, respectively. Cation disorder in the **I** block of the crystal structure of betalomonosovite results in doubling of the *b* unit-cell parameter and $b_{betalomo} = 2b_{lomo}$ (Table 1). The orientation of P tetrahedra, Na(3,4) and Na(5,6) octahedra along **b** in betalomonosovite supports the doubled *b* (*cf.* corresponding P tetrahedron, [8]-coordinated Na(1) polyhedron, and Na(3) octahedron in lomonosovite) (Fig. 7).

Microscale intergrowths

It is apparent from the detailed crystal structure of lomonosovite (Cámara *et al.* 2008) that lomonosovite contains neither H_2O nor OH groups. However, the infrared spectrum of lomonosovite (Figs. 1a, 1b) shows bands attributable to H_2O and OH (see discussion of the spectra above.) We concluded that these bands are due either to contamination or micro-intergrowths of an additional phase that contains H_2O and OH. The HRTEM results for lomonosovite (Fig. 4) show that lomonosovite indeed does contain micro-scale oriented intergrowths of an additional phase, and emphasize the need for complementary HRTEM examination of TS-block minerals when doing spectroscopic work.

The presence of $PO_3(OH)$ and $PO_2(OH)_2$ groups in betalomonosovite was originally proposed by Rastsvetaeva *et al.* (1975) and $PO_2(OH)_2$ groups alone by Rastsvetaeva (1986, 1988) and Khalilov (1990). Here, we have developed a model of the structure of betalomonosovite that contains both $PO_3(OH)$ and $PO_2(OH)_2$ groups, and provide spectroscopic evidence for the presence of both $PO_3(OH)$ and $PO_2(OH)_2$ groups (Fig. 2). Betalomonosovite also contains extensive micro-scale oriented intergrowths of an additional phase. Although this additional phase may be contributing signals to the infrared spectrum of betalomonosovite, the bond-lengths and bond valences of betalomonosovite (Tables 7 and 9) indicate the presence of both $PO_3(OH)$ and $PO_2(OH)_2$ groups in the betalomonosovite structure itself.

Related Minerals

Betalomonosovite is a Group-IV TS-block mineral. There are seven other minerals in this Group: murmanite, kolskyite, schüllerite, lomonosovite, quadruphite, sobolevite, and polyphite; they are listed in Table 1. In the structures of all eight Ti-disilicate minerals, the TS block exhibits linkage and stereochemistry typical of Group IV [Ti (+ Mg + Mn) = 4 *apfu*]: two H sheets connect to the O sheet such that two Si_2O_7 groups link to Ti polyhedra of the O sheet adjacent along $\mathbf{t_1}$. The crystal structure of lomonosovite is an alternation of TS and **I** blocks of the

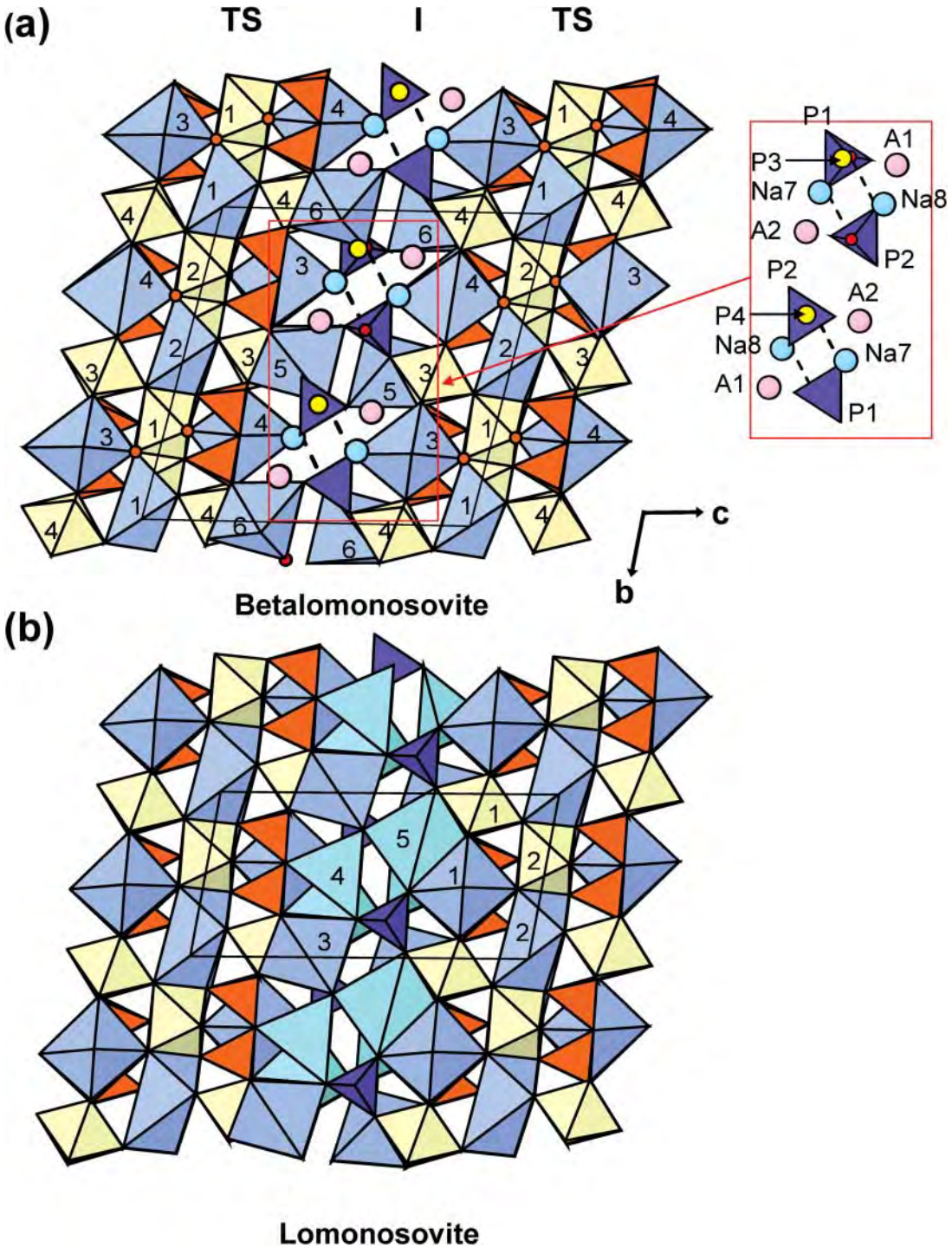

FIG. 7. General view of the crystal structures of (a) betalomonosovite and (b) lomonosovite. For betalomonosovite, cation polyhedra are shown for sites with more than 50% occupancy and atoms at sites with less than 50% occupancy are shown as spheres: A(1,2) – pink, Na(7,8) – blue, P(3,4) – yellow [see detailed labeling on the right from (a)]. Legend as in Figure 6a.

composition $Na_4Ti_4(Si_2O_7)_2O_4$ and $Na_6(PO_4)_2$, respectively. The crystal structure of betalomonosovite is of the same topology as that of lomonosovite and it is an alternation of TS and **I** blocks of the compositions $Na_4Ti_4(Si_2O_7)_2O_2(OF)$ and $Na_2\square_4[PO_3(OH)][PO_2(OH)_2]$, respectively. Betalomonosovite, $Na_6\square_4Ti_4(Si_2O_7)_2[PO_3(OH)][PO_2(OH)_2]O_2(OF)$ (Na = 6 *apfu*), is a Na-poor OH-bearing analogue of lomonosovite, $Na_{10}Ti_4(Si_2O_7)_2(PO_4)_2O_4$ (Na = 10 *apfu*). In the betalomonosovite structure, there is less Na in the **I** block and in the TS block when compared to the lomonosovite structure: in the **I** block, [4]-coordinated *Na*(7,8) and [5,6]-coordinated *A*(1,2) sites are 14% and 22% occupied by Na and Ca; in the TS block, [5]-coordinated *Na*(1,2) and [6]-coordinated *Na*(3,4) sites are 65% and 78% occupied by Na. OH groups occur in the TS block at the O(17,18) sites and in the **I** block where they coordinate P and Na atoms. The presence of OH groups in the TS block and **I** block of the betalomonosovite structure is supported by Raman and IR spectroscopy and bond-valence calculations on anions. We sum the monovalent anions at the O(17,18) sites, $F_{0.65}(OH)_{0.53}$, ideally F *apfu*, and in the **I** block, $(OH)_3$ *pfu*, to give a total of $(OH)_3F$ *pfu.* Hence the presence of four monovalent anions, $(OH)_3F$ *pfu*, compensates for the absence of four cations, Na_4 *pfu*, in the betalomonosovite structure. The ideal structural formula of betalomonosovite, $Na_2\square_4Na_2Ti_2Na_2Ti_2(Si_2O_7)_2[PO_3(OH)][PO_2(OH)_2]O_2(OF)$ is given in Table 1, and it is in close agreement with the ideal formula of Rastsvetaeva *et al.* (1975): $Na_2Ti_2[Na_2Ti_2Si_4]O_{18}Na_3[PO_3(OH)][PO_2(OH)_2]$. Betalomonosovite is the only Group-IV mineral that has $PO_3(OH)$ and $PO_2(OH)_2$ tetrahedra in the **I** block and OH groups in the TS block.

Summary

Betalomonosovite, ideally $Na_6\square_4Ti_4(Si_2O_7)_2[PO_3(OH)][PO_2(OH)_2]O_2(OF)$, is a Group-IV TS-block mineral (Ti + Mg + Mn = 4 *apfu*) in accord with Sokolova (2006). The crystal structure of betalomonosovite [*a* 5.3331(7), *b* 14.172(2), *c* 14.509(2) Å, α 103.174(2), β 96.320(2), γ 90.278(2)°, space group $P\bar{1}$, $Z = 2$] is an alternation of TS and **I** blocks of compositions $Na_4Ti_4(Si_2O_7)_2O_2(OF)$ and $Na_2\square_4[PO_3(OH)][PO_2(OH)_2]$, respectively. The crystal structure of betalomonosovite has the same topology as that of lomonosovite, $Na_{10}Ti_4(Si_2O_7)_2(PO_4)_2O_4$, with TS and **I** blocks of the composition $Na_4Ti_4(Si_2O_7)_2O_4$ and $Na_6(PO_4)_2$, respectively.

Betalomonosovite is a Na-poor OH-bearing analogue of lomonosovite. In the betalomonosovite structure, there is less Na in the in the **I** block and in the TS block when compared to the lomonosovite structure [*cf.* **I** block: $Na_2\square_4[PO_3(OH)][PO_2(OH)_2]$ (betalomonosovite) and $Na_6(PO_4)_2$ (lomonosovite)]. There is extensive cation and anion disorder in the crystal structure of betalomonosovite: in the **I** block, two *Na* sites are fully occupied and four alkali-cation sites are <50% occupied, and in the TS block, four *Na* sites have 65–78% occupancy.

To compensate for absence of Na, OH groups, and F atoms substitute for O atoms in the crystal structure of betalomonosovite. OH groups mainly occur in the **I** block where they coordinate P atoms to form $PO_3(OH)$ and $PO_2(OH)_2$ tetrahedra. OH groups also occur in the O sheet of the TS block where they are a part of two aggregate anions giving $O_{0.82}F_{0.65}(OH)_{0.53}$, ideally (OF) *apfu*. The presence of OH groups in the **I** block and in the TS block is supported by IR spectroscopy and bond-valence calculations for anions.

Acknowledgments

We thank Mark Welch for a thorough review of the manuscript and Editor Lee Groat for handling the review process. We are grateful to Mark Cooper for collecting experimental data on this very difficult material. We thank Mikhail E. Generalov and Vladimir Yu. Karpenko from the Fersman Mineralogical Museum, Moscow, Russia for the lomonosovite crystals from the holotype sample 42704 from Lovozero tundra, Kola Peninsula, Russia, and Kim Tait from the Royal Ontario Museum, Toronto, Canada, for the lomonosovite sample M36448 from the Khibiny alkaline massif, Kola Peninsula, Russia. This work was supported by a Canada Research Chair in Crystallography and Mineralogy and by a Discovery grant from the Natural Sciences and Engineering Research Council of Canada to FCH, and by Innovation Grants from the Canada Foundation for Innovation to FCH.

References

Ageeva, O.A. (1999) Typomorphism of accessory lomonosovite from rocks of Khibiny massif. *Zapiski Vserossiiskogo Mineralogicheskogo Obchshestva* **128(2)**, 99–104 (in Russian).

Aksenov, S.M., Rastsvetaeva, R.K., & Chukanov, N.V. (2014) The crystal structure of emmerichite $Ba_2Na_3Fe^{3+}Ti_2(Si_2O_7)_2O_2F_2$, a new lamprophyllite-group mineral. *Zeitschrift für Kristallographie* **229(1)**, 1–7.

Bellezza, M., Merlino, S., & Perchiazzi, N. (2009) Mosandrite, structural and crystal-chemical relationships with rinkite. *Canadian Mineralogist* **47**, 897–908.

Belov, N.V. & Organova, N.I. (1962) Crystal chemistry and mineralogy of the lomonosovite group in the light of the crystal structure of lomonosovite. *Geochemistry* N1, 4–13.

BELOV, N.V., GAVRILOVA, G.S., SOLOV'EVA, L.P., & KHALILOV, A.D. (1977) Refined structure of lomonosovite. *Soviet Physics Doklady* **22**, 422–424.

BROWN, I.D. (1981) The bond valence method: an empirical approach to chemical structure and bonding. *In* Structure and Bonding in Crystals II (M. O'Keeffe & A. Navrotsky, eds.). Academic Press, New York City, New York, United States (1–30).

BROWN, I.D. & ALTERMATT, D. (1985) Bond-valence parameters obtained from a systematic analysis of the inorganic crystal structure database. *Acta Crystallographica* **B41**, 244–247.

CÁMARA, F. & SOKOLOVA, E. (2007) From structure topology to chemical composition. VI. Titanium silicates: the crystal structure and crystal chemistry of bornemanite, a group-III Ti-disilicate mineral. *Mineralogical Magazine* **71**, 593–610.

CÁMARA, F. & SOKOLOVA, E. (2009) From structure topology to chemical composition. X. Titanium silicates: the crystal structure and crystal chemistry of nechelyustovite, a group III Ti-disilicate mineral. *Mineralogical Magazine* **73**, 887–897.

CÁMARA, F., SOKOLOVA, E., HAWTHORNE, F.C., & ABDU, Y. (2008) From structure topology to chemical composition. IX. Titanium silicates: revision of the crystal chemistry of lomonosovite and murmanite, Group-IV minerals. *Mineralogical Magazine* **72**, 1207–1228.

CÁMARA, F., SOKOLOVA, E., & NIETO, F. (2009) Cámaraite, $Ba_3NaTi_4(Fe^{2+},Mn)_8(Si_2O_7)_4O_4(OH,F)_7$. II. The crystal structure and crystal chemistry of a new group-II Ti-disilicate mineral. *Mineralogical Magazine* **73**, 855–870.

CÁMARA, F., SOKOLOVA, E., & HAWTHORNE, F.C. (2011) From structure topology to chemical composition. XII. Titanium silicates: the crystal chemistry of rinkite, Na_2Ca_4*REE*$Ti(Si_2O_7)_2OF_3$. *Mineralogical Magazine* **75**, 2755–2774.

CÁMARA, F., SOKOLOVA, E., & HAWTHORNE, F.C. (2012) Kazanskyite, $Ba□TiNbNa_3Ti(Si_2O_7)_2O_2(OH)_2(H2O)_4$, a Group-III Ti-disilicate mineral from the Khibiny alkaline massif, Kola Peninsula, Russia: description and crystal structure. *Mineralogical Magazine* **76**, 473–492.

CÁMARA, F., SOKOLOVA, E., ABDU, Y.A., HAWTHORNE, F.C., & KHOMYAKOV, A.P. (2013) Kolskyite, $(Ca□)Na_2Ti_4(Si_2O_7)_2O_4(H_2O)_7$, a Group-IV Ti-disilicate mineral from the Khibiny alkaline massif, Kola Peninsula, Russia: description and crystal structure. *Canadian Mineralogist* **51**, 921–936.

CÁMARA, F., SOKOLOVA, E., ABDU, Y.A., & HAWTHORNE, F.C. (2014) Saamite, $Ba□TiNbNa_3Ti(Si_2O_7)_2O_2(OH)_2(H_2O)_2$, a Group-III Ti-disilicate mineral from the Khibiny alkaline massif, Kola Peninsula, Russia: description and crystal structure. *Canadian Mineralogist* **52**, 745–761.

CHAPMAN, A.C. & THIRLWELL, L.E. (1964) Spectra of phosphorus compounds-I. The infra-red spectra of orthophosphates. *Spectrochimica Acta* **20**, 937–947.

CHUKANOV, N.V., RASTSVETAEVA, R.K., BRITVIN, S.N., VIRUS, A.A., BELAKOVSKIY, D.I., PEKOV, I.V., AKSENOV, S.M., & TERNES, B. (2011) Schüllerite, $Ba_2Na(Mn,Ca)(Fe^{3+},Mg,Fe^{2+})_2Ti_2(Si_2O_7)2(O,F)_4$, a new mineral from the Eifel volcanic region, Germany. *Zapiski Vserossiiskogo Mineralogicheskogo Obchshestva* **140(1)**, 67–75 (in Russian).

CHUKANOV, N.V., PEKOV, I.V., RASTSVETAEVA, R.K., AKSENOV, S.M., ZADOV, A.E., VAN, K.V., BLASS, G., SCHÜLLER, W., & TERNES, B. (2012) Lileyite, $Ba_2(Na,Fe,Ca)_3MgTi_2(Si_2O_7)_2O_2F_2$, a new lamprophyllite-group mineral from the Eifel volcanic area, Germany. *European Journal of Mineralogy* **24**, 181–188.

CHUKANOV, N.V., RASTSVETAEVA, R.K., AKSENOV, S.M., BLASS, G., PEKOV, I.V., BELAKOVSKIY, D.I., & TSCHÖRTNER, J. (2013) Emmerichite, IMA 2013-064. *Mineralogical Magazine* **77**, 2997–3005.

COOPER, M.A., HAWTHORNE, F.C., ABDU, Y.A., BALL, N.A., RAMIK, R.A., & TAIT, K.T. (2013) Wopmayite, ideally $Ca_6Na_3□Mn(PO_4)_3(PO_3OH)_4$, a new phosphate mineral from the Tanco Mine, Bernic Lake, Manitoba: description and crystal structure. *Canadian Mineralogist* **51**, 93–106.

FROST, R.L., LÓPEZ, A., THEISS, F.L., GRAÇA, L.M., & SCHOLZ, R. (2015) A vibrational spectroscopic study of the silicate mineral lomonosovite $Na_5Ti_2(Si_2O_7)(PO_4)O_2$. *Spectrochimica Acta Part A: Molecular and Biomolecular Spectroscopy* **134**, 53–57.

GENOVESE, A., CÁMARA, F., FALQUI, A., SOKOLOVA, E., & HAWTHORNE, F.C. (2014) HRTEM investigation of complex modular structures in geo-materials: an important investigation tool to reveal fine nanotextures of titanium-disilicates. 18th International Microscopy Congress, Abstracts, MS-13-P-2624. Prague, Czech Republic.

GERASIMOVSKIY, V.I. & KAZAKOVA, M.YE. (1962) Betalomonosovite. *Doklady Akademii Nauk SSSR, Earth Sciences* **142**, 118–121.

INTERNATIONAL TABLES FOR X-RAY CRYSTALLOGRAPHY (1992) *International Tables for X-Ray Crystallography*. V. C. Kluwer Academic Publishers, Dordrecht, Netherlands.

KHALILOV, A.D. (1990) Refinement of crystal structure of betalomonosovite from the Lovozero alkaline massif. *Mineralogicheskiy Zhurnal* **12(5)**, 10–18 (in Russian).

KHOMYAKOV, A.P. (1990) *Mineralogy of Hyperagpaitic Alkaline Rocks*. Nauka, Moscow, Russia, 144 pp. (in Russian).

LE CLÉAC'H, A. & GILLET, P. (1990) IR and Raman spectroscopic study of natural lawsonite. *European Journal of Mineralogy* **2**, 43–53.

LIBOWITZKY, E. (1999) Correlation of O-H stretching frequencies and O-H...O hydrogen bond lengths in minerals. *Monatshefte für Chemie* **130**, 1047–1059.

MORAES, A.P.A., ROMANO, R., SOUZA FILHO, A.G., FREIRE, P. T.C., MENDES FILHO, J., & ALVES, O.L. (2006) Vibrational spectra of α-$Ge(HPO_4)_2.H_2O$ compound. *Vibrational Spectroscopy* **40**, 209–212.

POUCHOU, J.L. & PICHOIR, F. (1985) 'PAP' φ(ρZ) procedure for improved quantitative microanalysis. *In* Microbeam Analysis (J.T. Armstrong, ed.). San Francisco Press, San Francisco, California (104–106).

RASTSVETAEVA, R.K. (1986) Crystal structure of betalomonosovite from the Lovozero region. *Soviet Physics Crystallography* **31**, 633–636.

RASTSVETAEVA, R.K. (1988) Crystal structure of the disordered modification of betalomonosovite. *Zapiski Vsesoyuznogo Mineralogicheskogo Obchshestva* **117(6)**, 696–705 (in Russian).

RASTSVETAEVA, R.K. (1989) On structure transformations in betalomonosovite. *Kristallografiya* **34**, 880–884 (in Russian).

RASTSVETAEVA, R.K., SIROTA, M.I., & BELOV, N.V. (1975) Crystal structure of betalomonosovite. *Soviet Physics Crystallography* **20**, 158–160.

RASTSVETAEVA, R.K., AKSENOV, S.M., & CHUKANOV, N.V. (2011) Crystal structure of schüllerite, a new mineral of the heterophyllosilicate family. *Doklady Chemistry* **437**, 90–94.

SEMENOV, E.I., ORGANOVA, N.I., & KUCHARCHIK, M.V. (1961) New data on the minerals of the lomonosovite-murmanite group. *Kristallografiya* **6**, 925–932 (in Russian).

SHANNON, R.D. (1976) Revised effective ionic radii and systematic studies of interatomic distances in halides and chalcogenides. *Acta Crystallographica* **A32**, 751–767.

SHELDRICK, G.M. (2008) A short history of SHELX. *Acta Crystallographica* **A64**, 112–122.

SOKOLOVA, E. (2006) From structure topology to chemical composition. I. Structural hierarchy and stereochemistry in titanium disilicate minerals. *Canadian Mineralogist* **44**, 1273–1330.

SOKOLOVA, E. & CÁMARA, F. (2007) From structure topology to chemical composition. II. Titanium silicates: revision of the crystal structure and chemical formula of delindeite. *Canadian Mineralogist* **45**, 1247–1261.

SOKOLOVA, E. & CÁMARA, F. (2008) From structure topology to chemical composition. III. Titanium silicates: crystal chemistry of barytolamprophyllite. *Canadian Mineralogist* **46**, 403–412.

SOKOLOVA, E. & CÁMARA, F. (2013) From structure topology to chemical composition. XVI. New developments in the crystal chemistry and prediction of new structure topologies for titanium disilicate minerals with the TS block. *Canadian Mineralogist* **51**, 861–891.

SOKOLOVA, E. & CÁMARA, F. (2014) From structure topology to chemical composition. XVII. Fe^{3+} versus Ti^{4+}: The topology of the HOH layer in ericssonite-2*O*, $Ba_2Fe^{3+}{}_2Mn_4(Si_2O_7)_2O_2(OH)_2$, ferroericssonite, $Ba_2Fe^{3+}{}_2Fe^{2+}{}_4(Si_2O_7)_2O_2(OH)_2$, and yoshimuraite, $Ba_4Ti^{4+}{}_2Mn_4(Si_2O_7)_2(PO_4)_2O_2(OH)_2$. *Canadian Mineralogist* **52**, 569–576.

SOKOLOVA, E. & HAWTHORNE, F.C. (2001) The crystal chemistry of the $[M_3O_{11\text{-}14}]$ trimeric structures: from hyperagpaitic complexes to saline lakes. *Canadian Mineralogist* **39**, 1275–1294.

SOKOLOVA, E. & HAWTHORNE, F.C. (2008a) From structure topology to chemical composition. IV. Titanium silicates: the orthorhombic polytype of nabalamprophyllite from Lovozero massif, Kola Peninsula, Russia. *Canadian Mineralogist* **46**, 1323–1331.

SOKOLOVA, E. & HAWTHORNE, F.C. (2008b) From structure topology to chemical composition. V. Titanium silicates: crystal chemistry of nacareniobsite-(Ce). *Canadian Mineralogist* **46**, 1333–1342.

SOKOLOVA, E. & HAWTHORNE, F.C. (2013) From structure topology to chemical composition. XIV. Titanium silicates: refinement of the crystal structure and revision of the chemical formula of mosandrite, $(Ca_3\textit{REE})[(H_2O)_2Ca_{0.5}\square_{0.5}]Ti(Si_2O_7)_2(OH)_2(H_2O)_2$, a Group-I mineral from the Saga mine, Morje, Porsgrunn, Norway. *Mineralogical Magazine* **77**, 2753–2771.

SOKOLOVA, E., HAWTHORNE, F.C., & KHOMYAKOV, A.P. (2005) Polyphite and sobolevite: revision of their crystal structures. *Canadian Mineralogist* **43**, 1527–1544.

SOKOLOVA, E., ABDU, Y., HAWTHORNE, F.C., STEPANOV, A.V., BEKENOVA, G.K., & KOTEL'NIKOV, P.E. (2009a) Cámaraite, $Ba_3NaTi_4(Fe^{2+},Mn)_8(Si_2O_7)_4O_4(OH,F)_7$. I. A new titanium-silicate mineral from the Verkhnee Espe deposit, Akjailyautas Mountains, Kazakhstan. *Mineralogical Magazine* **73**, 847–854.

SOKOLOVA, E., CÁMARA, F., HAWTHORNE, F.C., & ABDU, Y. (2009b) From structure topology to chemical composition. VII. Titanium silicates: the crystal structure and crystal chemistry of jinshajiangite. *European Journal of Mineralogy* **21**, 871–883.

SOKOLOVA, E., CÁMARA, F., & HAWTHORNE, F.C. (2011) From structure topology to chemical composition. XI. Titanium silicates: crystal structures of innelite-1*T* and innelite-2*M* from Inagli massif, Yakutia, Russia, and the crystal chemistry of innelite. *Mineralogical Magazine* **75**, 2495–2518.

Sokolova, E., Hawthorne, F.C., & Abdu, Y.A. (2013) From structure topology to chemical composition. XV. Titanium silicates: revision of the crystal structure and chemical formula of schüllerite, $Na_2Ba_2Mg_2Ti_2(Si_2O_7)_2O_2F_2$, from the Eifel volcanic region, Germany. *Canadian Mineralogist* **51**, 715–725.

Sokolova, E., Cámara, F., Hawthorne, F.C., Horváth, L., & Pfenninger-Horváth, E. (2014) Bobshannonite, IMA 2014-052. *Mineralogical Magazine* **78**, 1241–1248.

Taher, L.B., Smiri, L., & Bulou, A. (2001) Investigation of mixed divalent cation monophosphates: Synthesis, crystal structure, and vibrational study of $CdBa_2(HPO_4)_2(H_2PO_4)_2$. *Journal of Solid State Chemistry* **161**, 97–105.

Wojdyr, M. (2010) Fityk: a general-purpose peak fitting program. *Journal of Applied Crystallography* **43**, 1126–1128.

Received May 22, 2014, revised manuscript accepted April 21, 2015.